

Quark mass effects in two-loop Higgs amplitudes

Charalampos Anastasiou¹, Nicolas Deutschmann¹, and Armin Schweitzer¹

¹*ETH Zürich, Rämistrasse 101, 8092 Zürich, Switzerland*

Abstract

We provide two two-loop amplitudes relevant for precision Higgs physics. The first is the two-loop amplitude for Higgs boson production through gluon fusion with exact dependence on the top quark mass up to squared order in the dimensional regulator ε . The second result we provide is the two-loop amplitude for the decay of a Higgs boson into a pair of massive bottom quarks through the Higgs-to-gluon coupling in the infinite top mass limit. Both amplitudes are computed by finding canonical bases of master integrals, which we evaluate explicitly in terms of harmonic polylogarithms. We obtain the bare, renormalized and IR-subtracted amplitude and provide the results in terms of building blocks suitable for changing renormalization schemes.

Contents

| | | |
|----------|--|-----------|
| 1 | Introduction | 3 |
| 2 | Amplitudes and results for $gg \rightarrow H$ | 5 |
| 2.1 | Notation for bare amplitudes | 5 |
| 2.2 | Renormalization and IR-subtraction | 6 |
| 2.3 | Kinematic limits | 8 |
| 3 | Amplitudes and results for $H \rightarrow b\bar{b}$ | 12 |
| 3.1 | Higgs effective field theory | 12 |
| 3.2 | Notation for bare amplitudes | 13 |
| 3.3 | Renormalization and IR-subtraction | 16 |
| 3.4 | Small mass expansion | 18 |
| 4 | Analytic continuation for $gg \rightarrow H$ and $H \rightarrow b\bar{b}$ | 18 |
| 5 | Computation of master integrals | 20 |
| 5.1 | Master integrals for M_{LO}^0 in $gg \rightarrow H$ | 21 |
| 5.2 | Master integrals for M_{NLO}^0 in $gg \rightarrow H$ | 22 |
| 5.3 | One-Loop master integrals in $H \rightarrow b\bar{b}$ | 24 |
| 5.4 | Two-Loop master integrals in $H \rightarrow b\bar{b}$ | 25 |
| 6 | Conclusion | 29 |
| | Appendix A Tensor basis for the $H \rightarrow b\bar{b}$ amplitude | 30 |

1 Introduction

The Run II of the LHC has allowed experimental collaborations to probe the Higgs boson to unprecedented levels of precision. Recent combination results by CMS [1] and ATLAS [2] show a 60% reduction in the global signal strength compared to the historic Run I combinations. Run II has also seen impressive developments in differential observables [3, 4] which can provide rich information on the dynamics of the Higgs boson.

As a result of this steady experimental progress, making precise theoretical predictions of the relevant observables is highly important as their comparison to measurements will allow us to test the Standard Model and highlight possible new physics through any discrepancy.

Intense theoretical effort has been devoted to making such highly precise predictions of Higgs observables. The inclusive cross section was obtained at next-to-next-to-next-to-leading order (N^3LO) in the QCD coupling using the Higgs Effective Theory (HEFT) where the top quark is infinitely massive [5]. Approximated Higgs-boson rapidity distributions were also obtained at N^3LO [6, 7].

The infinite top mass approximation has a $\sim 6\%$ effect on the cross section, estimated from the NLO [8] prediction, which is applied to the state-of-the-art N^3LO through a multiplicative correction factor. The finite-mass corrections mostly factorize from the perturbative corrections [5], so that rescaling by known exact results induces only an estimated $\sim 1\%$ uncertainty on the prediction [9, 10]. At the inclusive level, the uncertainty associated to this rescaling constitutes therefore a sizeable portion of the $\sim 5\%$ theoretical error. At the differential level, mass effects are all the more important in the high energy region where the HEFT has been shown to fail by the first exact NLO prediction of the Higgs boson transverse momentum (p_T) [11]. While this work also highlighted that more refined approaches such as the FT_{approx} description can provide a reasonable description within 10% up to high energies, the projected $\sim 5\%$ uncertainty of future HL-LHC transverse momentum spectrum measurements [12, 13] warrants turning our sights toward a better control of mass effects in Higgs physics predictions. This situation could be improved by computing the NNLO hadronic Higgs boson cross section including exact top-mass effects.

This goal is becoming realistic thanks to the recent derivation of the three-loop double-virtual contribution, which started with an approximate result extrapolating expansions in multiple regimes [14]. The light-fermion contributions with exact top mass dependence were then obtained [15], followed by the numerical evaluation of the complete result [16]. Combined with the knowledge of all integrals of the two-loop real-virtual contributions [17–19], a full prediction is now within reach.

Motivated by this situation, the first part of this paper provides the analytic result for the two-loop amplitude for the process $gg \rightarrow H$ to order $\mathcal{O}(\varepsilon^2)$, which is required to build the infrared (IR) subtraction terms of the double-virtual contribution. These were used in [16] to obtain a finite remainder but are not publicly available.

Probing rare production channels beyond the dominant top-loop mediated process is instrumental to a comprehensive study of the interactions of the Higgs boson with other Standard Model particles. Weak production modes such as Higgstrahlung (VH) provide key insights to test our understanding of electroweak symmetry breaking as well as a window into the Higgs to bottom quark decay channel, which is otherwise dominated by QCD backgrounds [20, 21].

The current uncertainties do not qualify this process as a precision observable, but statistics will significantly improve the situation [22] to a point where theory uncertainties are expected to dominate. The current theoretical state-of-the-art predictions [23, 24] combine NNLO predictions for the production [25, 26] and the decay [27, 28] fully differentially. This work has shown that even the pure NNLO correction to the decay can have large effects on differential observables, which motivates improving our description of the decay of the Higgs boson to a pair of bottom quarks ($H \rightarrow b\bar{b}$).

The current state-of-the-art prediction for the $H \rightarrow b\bar{b}$ decay is N⁴LO at the fully inclusive level [29] and N³LO at the differential level [30]. These predictions are made in the limit where the bottom quark is massless and therefore neglect contributions from top-quark loops induced by the top-quark Yukawa coupling. These appear at NNLO and generate difficulty to treat infrared divergences in the massless bottom-quark limit [24]. This difficulty means that the state-of-the-art predictions for $VH, H \rightarrow b\bar{b}$ [23, 24], which rely on massless bottom NNLO calculations [27, 28] also miss these contributions. Top-induced effects are currently untractable in massless bottom calculations, so that they can only be obtained by performing the calculation of the Higgs decay into massive bottom quarks. This was completed at NNLO [31, 32] and included a HEFT description¹ of the first non-zero top quark effects. This work highlighted that the top-induced contributions have an impact of around 2% on the Higgs width through their interference with the leading process and therefore contribute about 25% of the pure NNLO effects. In order to further improve our control of the $H \rightarrow b\bar{b}$ decay, it is desirable to compute the top-induced N³LO effects in the HEFT. This is the first order at which squared top-induced processes occur, which we can straightforwardly compute using automated tools such as MG5_aMC@NLO [34]. At the inclusive level, these squared contributions have an effect of about 1% on the decay width, making them dominant over the existing N³LO prediction, which are of around 0.2% [29], motivating the derivation complete the N³LO top-induced contributions. The missing piece of this calculation is the two-loop amplitude for the decay of a Higgs boson to a pair of massive bottom quarks mediated by the Higgs-to-gluon coupling in the HEFT, which we provide in the second part of this paper.

This paper is organized in the following way. Section 2 presents the calculation of the one and two-loop amplitudes for gluon-fusion Higgs production to high order in the dimensional regulator and provides the results and their expansions in two kinematic limits. Section 3

¹The HEFT description of top-induced $H \rightarrow b\bar{b}$ was found to be extremely accurate by comparing to the exact calculation [33]

presents the same results for the one and two-loop amplitudes that contribute to the top-quark-Yukawa-induced Higgs to bottom decay. We subsequently discuss the analytic continuation of the result in section 4 and finally discuss the details of the computation of the master integrals (MIs) in section 5.

2 Amplitudes and results for $gg \rightarrow H$

2.1 Notation for bare amplitudes

The bare amplitude $\mathcal{A}_{gg \rightarrow H}^0$ of the process $g(p_1)g(p_2) \rightarrow H$ can be written as

$$\begin{aligned} \mathcal{A}_{gg \rightarrow H}^0 &= \frac{2i}{v^0} \frac{\alpha_s^0 S_\varepsilon \mu^{-2\varepsilon}}{4\pi} \left(-\frac{s}{\mu^2} \right)^{-\varepsilon} \delta_{ab} (s (\varepsilon_1 \cdot \varepsilon_2) - 2 (\varepsilon_1 \cdot p_2) (\varepsilon_2 \cdot p_1)) \\ &\times \left(M_{\text{LO}}^0 + \frac{\alpha_s^0 S_\varepsilon \mu^{-2\varepsilon}}{4\pi} \left(-\frac{s}{\mu^2} \right)^{-\varepsilon} M_{\text{NLO}}^0 + \mathcal{O}((\alpha_s^0)^3) \right), \end{aligned} \quad (2.1)$$

where $s = (p_1 + p_2)^2 = m_H^2$,

$$S_\varepsilon = (4\pi)^\varepsilon \exp(-\varepsilon \gamma_E) \quad (2.2)$$

and v^0 denotes the bare vacuum expectation value. The gluons are in physical gauge with $\varepsilon_i(p_i) \cdot p_i = 0$.

In order to compute the form factors M_X^0 , we first generate all contributing diagrams with QGRAF [35] and perform the color-, Dirac- and Lorentz algebra in Mathematica. Traces of γ matrix chains are performed with FORM [36]. The integration-by-parts (IBP) reductions [37, 38] to scalar master integrals (MIs) are done with the programs AIR [39] and KIRA [40].

We separate M_{NLO}^0 according to

$$M_{\text{NLO}}^0 = M_{\text{UV},m}^0 + M_{\text{uv}}^0 + M_{\text{IR}}^0 + \log \left(-\frac{s}{\mu^2} \right) M_{\text{fin,scale}}^0 + M_{\text{fin}}^0, \quad (2.3)$$

where infrared singularities are isolated in M_{IR}^0 and ultraviolet poles are contained in M_{UV}^0 and $M_{\text{UV},m}^0$, respectively harboring terms renormalized by coupling and mass counterterms. Of the two remaining regular terms, $M_{\text{fin,scale}}^0$ contains the complete dependence on the renormalization scale μ^2 while M_{fin}^0 corresponds to the case of $\mu^2 = m_H^2$. We have

$$M_{\text{UV}}^0 = \frac{\beta_0}{\varepsilon} \left(-\frac{s}{\mu^2} \right)^\varepsilon M_{\text{LO}}^0, \quad (2.4)$$

$$M_{\text{UV},m}^0 = \frac{6}{\varepsilon} C_F \left(-\frac{s}{\mu^2} \right)^\varepsilon (m_t^0)^2 \frac{\partial}{\partial (m_t^0)^2} M_{\text{LO}}^0, \quad (2.5)$$

$$\begin{aligned} M_{\text{IR}}^0 &= \left(-\frac{s}{\mu^2} \right)^\varepsilon \mathcal{I}_1 M_{\text{LO}}^0 \\ &= -\frac{e^{\gamma_E \varepsilon}}{\Gamma(1-\varepsilon)} \left(\frac{\beta_0}{\varepsilon} + \frac{2N_c}{\varepsilon^2} \right) M_{\text{LO}}^0 \end{aligned} \quad (2.6)$$

with

$$\beta_0 = \frac{11N_c}{3} - \frac{2N_f}{3}, \quad N_f = 5 \quad \text{and} \quad C_F = (N_c^2 - 1)/(2N_c). \quad (2.7)$$

We checked the bare LO and NLO against [8] by inserting our expressions into their eq (7.4). We furthermore compared the ε^0 of M_{NLO}^0 against [41] and the analytic expression implemented in the program iHixs 2 [42]². We find full agreement in all cases³.

The higher orders in ε of the amplitude (2.1) are very cumbersome. We therefore only report their expansion in kinematics limits here and provide the exact results as ancillary files.

2.2 Renormalization and IR-subtraction

The renormalized amplitude reads

$$\mathcal{A}(\alpha_s, m_t, \mu) = Z_g \mathcal{A}^0(\alpha_s^0, m_t^0), \quad (2.8)$$

where Z_g denotes the gluon wave-function renormalization function, μ the renormalization scale and the superscript 0 indicates bare quantities. The renormalized parameters are related to the bare ones by:

$$\alpha_s^0 = \frac{\mu^{2\varepsilon}}{S_\varepsilon} Z_{\alpha_s} \alpha_s, \quad m_t^0 = Z_m m_t, \quad v^0 = \mu^{-\varepsilon} v, \quad (2.9)$$

and we define the bare Yukawa coupling by its relation to other parameters: $y_t^0 = m_t^0/v^0$.

We renormalize the strong coupling and the gluon field in a mixed scheme with $N_f = 5$ light flavours, whose contributions are subtracted in $\overline{\text{MS}}$ while contributions involving the top-quark are renormalized on-shell, at zero momentum [45]. This yields

$$Z_{\alpha_s} = 1 - \frac{\alpha_s}{4\pi} \frac{1}{\varepsilon} \left(\beta_0 - \frac{2}{3} \left(\frac{\mu^2}{m_t^2} \right)^\varepsilon \right) \quad (2.10)$$

and

$$Z_g = 1 + \frac{\alpha_s}{4\pi} \frac{2}{3\varepsilon} \left(\frac{\mu^2}{m_t^2} \right)^\varepsilon. \quad (2.11)$$

For the sake of more compact expressions we renormalize the top mass in $\overline{\text{MS}}$:

$$Z_m = 1 - \frac{\alpha_s}{4\pi} C_F \frac{3}{\varepsilon}. \quad (2.12)$$

Note that these choices are such that the counterterms generated by eq. (2.11) and eq. (2.12) cancel the UV terms in the bare amplitude of eq. (2.3) up to neglected orders in α_s but to all orders in ε :

$$M_{\text{NLO}} = M_{\text{NLO}}^0 - M_{\text{UV}}^0 - M_{\text{UV},m}^0 + \mathcal{O}(\alpha_s), \quad (2.13)$$

²see: https://github.com/dulatf/iHixs/blob/master/src/higgs/exact_qcd_corrections/nlo_exact_matrix_elements.cpp and function `ggf_exact_virtual_ep0` therein.

³The comparison with iHIXS 2 requires the subtraction of IR divergences with $\tilde{I}_1 = -\frac{e^{\gamma_E \varepsilon}}{\Gamma(1-\varepsilon)} \left(\frac{\beta_0}{\varepsilon} + \frac{2N_c}{\varepsilon^2} \left(-\frac{s}{\mu^2} \right)^{-\varepsilon} \right)$ as defined in e.g. [43] or [44] removing the β_0 dependence in M_{fin}^0 .

where we exploit the fact that $m_t^0 - m_t = \mathcal{O}(\alpha_s)$ can be neglected at this order.

The renormalized amplitude still features poles in ε that are of infrared and collinear origin. These singularities have a universal structure in that it can be expressed in a factorized fashion using lower orders of the amplitude [43, 44]:

$$M_{\text{NLO}} = F_{\text{NLO}} + \mathcal{I}_1 M_{\text{LO}}, \quad (2.14)$$

where F_{NLO} is finite and M_{LO} is the renormalized leading-order scalar amplitude, which in our case is trivially obtained by replacing m_t^0 by m_t in M_{LO}^0 . Again, our splitting of the bare amplitude in eq. (2.3) is such that the IR subtraction term cancels M_{IR}^0 to all orders in ε and to all relevant orders in α_s so that

$$F_{\text{NLO}} = M_{\text{NLO}} - M_{\text{IR}}^0 + \mathcal{O}(\alpha_s) \quad (2.15)$$

$$= \log\left(-\frac{s}{\mu^2}\right) M_{\text{fin, scale}} + M_{\text{fin}}, \quad (2.16)$$

where $M_{\text{fin, scale}}$ and M_{fin} are obtained from $M_{\text{fin, scale}}^0$ and M_{fin}^0 by substituting m_t^0 with m_t .

The complete renormalized and IR-subtracted NLO-contribution to $gg \rightarrow H$ in the above discussed schemes is simply given by

$$\begin{aligned} A_{gg \rightarrow H}^{\text{NLO}, F} &= \frac{2i}{v} \frac{\alpha_s}{4\pi} \left(-\frac{s}{\mu^2}\right)^{-2\varepsilon} \delta_{ab} (s(\varepsilon_1 \cdot \varepsilon_2) - 2(\varepsilon_1 \cdot p_2)(\varepsilon_2 \cdot p_1)) \\ &\times \left(\log\left(-\frac{s}{\mu^2}\right) M_{\text{fin, scale}} + M_{\text{fin}} \right). \end{aligned} \quad (2.17)$$

The artificial splitting of the bare amplitude in (2.1) and the corresponding ancillary material is designed to make changes of renormalization or IR-subtraction schemes particularly simple. A change of renormalization schemes, e.g. to the on-shell scheme for the top mass renormalization with

$$Z_m^{\text{OS}} = 1 + \frac{\alpha_s}{4\pi} \delta Z_m^{\text{OS}} \quad (2.18)$$

can straightforwardly be obtained by computing the corresponding finite piece

$$\Delta M_{\text{UV}, m} = \left(-\frac{s}{\mu^2}\right)^{\varepsilon} \left(-2(m_t)^2 (\delta Z_m^{\text{OS}} - \delta Z_m) \frac{\partial}{\partial (m_t^0)^2} M_{\text{LO}} \right), \quad (2.19)$$

and adding it to the $\overline{\text{MS}}$ renormalized NLO piece in (2.17) obtaining

$$\begin{aligned} A_{gg \rightarrow H}^{\text{NLO}, \text{OS}} &= \frac{2i}{v} \frac{\alpha_s}{4\pi} \left(-\frac{s}{\mu^2}\right)^{-2\varepsilon} \delta_{ab} (s(\varepsilon_1 \cdot \varepsilon_2) - 2(\varepsilon_1 \cdot p_2)(\varepsilon_2 \cdot p_1)) \\ &\times \left(\log\left(-\frac{s}{\mu^2}\right) M_{\text{fin, scale}} + M_{\text{fin}} + \Delta M_{\text{UV}, m} \right). \end{aligned} \quad (2.20)$$

2.3 Kinematic limits

In the following we discuss the amplitude in the limits $|s| \gg m_t^2$ and $|s| \ll m_t^2$. The second limit in particular can be used as an important check of the full result since it has a direct correspondence to the heavy top EFT, in which the inclusive cross-section of $gg \rightarrow H$ is known to N³LO [5, 46]. The small mass limit was obtained up to finite order in the dimensional regulator in [47].

2.3.1 Small mass expansion

We perform the expansion around the limit $m_t \rightarrow 0$ (or $|s| \rightarrow \infty$) with the code POLYLOG-TOOLS [48] in the Euclidean regime and find for the leading order contribution

$$\begin{aligned}
-\frac{2m_t^2}{s} M_{\text{LO}}^{0,m_t \rightarrow 0} = & 1 - \frac{\log^2(x)}{4} + \varepsilon \left[\frac{\log^3(x)}{6} + \frac{1}{12} \pi^2 \log(x) + \frac{3(\zeta_3 + 2)}{2} \right] \\
& + \varepsilon^2 \left[-\frac{1}{2} \zeta_3 \log(x) - \frac{1}{16} \log^4(x) - \frac{1}{16} \pi^2 \log^2(x) + \frac{1}{144} \pi^2 (\pi^2 - 12) + 7 \right] \\
& + \varepsilon^3 \left[\frac{1}{3} \zeta_3 \log^2(x) + \frac{\log^5(x)}{60} + \frac{1}{36} \pi^2 \log^3(x) + \frac{1}{80} \pi^4 \log(x) \right. \\
& \quad \left. + \frac{7\zeta_5}{2} - \frac{1}{24} \pi^2 (\zeta_3 + 6) - \frac{7\zeta_3}{3} + 15 \right] \\
& + \varepsilon^4 \left[-\frac{5}{36} \zeta_3 \log^3(x) + \left(-\frac{5\pi^2 \zeta_3}{72} - \frac{\zeta_5}{2} \right) \log(x) - \frac{1}{288} \log^6(x) \right. \\
& \quad - \frac{5}{576} \pi^2 \log^4(x) - \frac{1}{128} \pi^4 \log^2(x) - \frac{3\zeta_3^2}{2} \\
& \quad \left. - 7\zeta_3 + \frac{\pi^2 (-5040 - 282\pi^2 + 23\pi^4)}{8640} + 31 \right] + \mathcal{O}(\varepsilon^5) . \tag{2.21}
\end{aligned}$$

The NLO pieces in (2.1) expanded in the limit of a small top-mass are

$$\begin{aligned}
-\frac{2m_t^2}{s} M_{\text{NLO}}^{0,m_t \rightarrow 0} = & \frac{1}{\varepsilon^2} \left[-6 + \frac{3 \log^2(x)}{2} \right] \\
& + \frac{1}{\varepsilon} \left[-\log^3(x) - 2 \log^2(x) + \left(-4 - \frac{\pi^2}{2} \right) \log(x) - 9\zeta_3 - 10 \right] \\
& + \left[\frac{1}{9} (-39\zeta_3 - 48 + 10\pi^2) \log(x) + \frac{11 \log^4(x)}{36} + \frac{8 \log^3(x)}{3} \right. \\
& \quad \left. + \left(\frac{23}{6} + \frac{7\pi^2}{36} \right) \log^2(x) - \frac{26\zeta_3}{3} - \frac{7\pi^4}{40} + \frac{5\pi^2}{3} + 24 \right] \\
& + \varepsilon \left[\frac{\log^2(x)}{9} (-33\zeta_3 + 21 - 11\pi^2) - \frac{\log^5(x)}{60} - 2 \log^4(x) \right. \\
& \quad + \frac{1}{18} (-41 - \pi^2) \log^3(x) + \frac{\log(x)}{54} (-612\zeta_3 - 576 - 15\pi^2 - 8\pi^4) \\
& \quad \left. - \frac{116\zeta_5}{3} + \frac{1}{3} (19\pi^2 - 173) \zeta_3 - \frac{68\pi^4}{135} + 244 \right]
\end{aligned}$$

$$\begin{aligned}
& + \varepsilon^2 \left[\frac{\log^3(x)}{9} (43\zeta_3 + 7 + 8\pi^2) + \frac{\log^2(x)}{144} (96(17\zeta_3 + 7) + 92\pi^2 + 19\pi^4) \right. \\
& + \frac{\log(x)}{270} (-75\pi^2(\zeta_3 + 2) - 90(6\zeta_3 - 163\zeta_5 + 64) + 94\pi^4) \\
& - \frac{7\log^6(x)}{216} + \frac{16\log^5(x)}{15} + \frac{1}{216} (219 + 5\pi^2) \log^4(x) - 60\zeta_5 \\
& + \frac{\zeta_3}{6} (1235\zeta_3 - 2348) + \frac{\pi^2}{9} (52\zeta_3 - 147) + \frac{6617\pi^6}{27216} \\
& \left. - \frac{1559\pi^4}{1080} + 1192 \right] + \mathcal{O}(\varepsilon^3) \tag{2.22}
\end{aligned}$$

and in particular

$$\begin{aligned}
-\frac{2m_t^2}{s} M_{\text{fin}}^{0,m_t \rightarrow 0} &= \frac{2}{9} (-33\zeta_3 - 24 + 2\pi^2) \log(x) - \frac{5}{72} \log^4(x) + \frac{4\log^3(x)}{3} \\
&+ \frac{1}{18} (-3 - \pi^2) \log^2(x) - \frac{2}{15} (155\zeta_3 - 315 + \pi^4) \\
&+ \varepsilon \left[\beta_0 \left(\frac{1}{48} \pi^2 \log^2(x) - \frac{\pi^2}{12} \right) + \frac{1}{18} (-21\zeta_3 + 42 - 13\pi^2) \log^2(x) \right. \\
&+ \frac{1}{270} (-180(11\zeta_3 + 16) + 195\pi^2 - 31\pi^4) \log(x) + \frac{\log^5(x)}{12} \\
&- \frac{3\log^4(x)}{2} + \frac{1}{36} (\pi^2 - 10) \log^3(x) + \frac{1}{3} (-209\zeta_3 - 53\zeta_5 + 834) \\
&\left. + \frac{1}{3} \pi^2 (16\zeta_3 - 7) - \frac{151\pi^4}{270} \right] \\
&+ \varepsilon^2 \left[\beta_0 \left(\frac{1}{12} \zeta_3 \log^2(x) - \frac{1}{72} \pi^2 \log^3(x) - \frac{1}{144} \pi^4 \log(x) - \frac{1}{8} \pi^2 (\zeta_3 + 2) - \frac{\zeta_3}{3} \right) \right. \\
&+ \frac{1}{18} (65\zeta_3 + 14 + 12\pi^2) \log^3(x) \\
&+ \frac{1}{720} (480(13\zeta_3 + 7) - 20\pi^2 + 83\pi^4) \log^2(x) \\
&+ \frac{1}{270} (-15\pi^2(11\zeta_3 + 10) - 180(11\zeta_3 - 77\zeta_5 + 32) + 67\pi^4) \log(x) \\
&- \frac{23}{432} \log^6(x) + \frac{14\log^5(x)}{15} + \frac{1}{432} (150 + \pi^2) \log^4(x) - 88\zeta_5 \\
&+ \frac{1}{6} \zeta_3 (1163\zeta_3 - 2524) + \frac{1}{9} \pi^2 (55\zeta_3 - 192) + \frac{17393\pi^6}{68040} \\
&\left. - \frac{1829\pi^4}{1080} + 1258 \right] + \mathcal{O}(\varepsilon^3) \tag{2.23}
\end{aligned}$$

and

$$\begin{aligned}
-\frac{2m_t^2}{s} M_{\text{fin,scale}}^{0,m_t \rightarrow 0} &= -\beta_0 + \frac{1}{4} (\beta_0 + 8) \log^2(x) + 4 \log(x) - 8 \\
&+ \varepsilon \left[-3\beta_0 + \log \left(-\frac{s}{\mu^2} \right) \left(-\frac{\beta_0}{2} + \frac{1}{8} (\beta_0 + 8) \log^2(x) + 2 \log(x) - 4 \right) \right. \\
&\left. + \frac{1}{6} (-\beta_0 - 8) \log^3(x) - \frac{1}{12} \pi^2 (\beta_0 + 8) \log(x) - 4 \log^2(x) \right]
\end{aligned}$$

$$\begin{aligned}
& -\frac{3}{2}(\beta_0 + 8)\zeta(3) - \frac{2\pi^2}{3} - 24 \Big] \\
& + \varepsilon^2 \Big[-\frac{1}{144}(1008 - 12\pi^2 + \pi^4)(\beta_0 + 8) \\
& + \log^2\left(-\frac{s}{\mu^2}\right) \left(\frac{1}{6}(-\beta_0 - 8) + \frac{1}{24}(\beta_0 + 8)\log^2(x) + \frac{2\log(x)}{3} \right) \\
& + \log\left(-\frac{s}{\mu^2}\right) \left(\frac{1}{12}(-\beta_0 - 8)\log^3(x) - \frac{1}{24}\pi^2(\beta_0 + 8)\log(x) \right. \\
& \quad \left. - 2\log^2(x) - \frac{3}{4}\beta_0(\zeta(3) + 2) - 6(\zeta(3) + 2) - \frac{\pi^2}{3} \right) \\
& + \frac{1}{16}(\beta_0 + 8)\log^4(x) + \frac{1}{16}\pi^2(\beta_0 + 8)\log^2(x) \\
& + \log(x) \left(\frac{1}{2}(\beta_0 + 8)\zeta(3) + \pi^2 \right) + 2\log^3(x) + 4\zeta(3) \Big] \\
& + \mathcal{O}(\varepsilon^3)
\end{aligned} \tag{2.24}$$

where $\log(x) = -\log(-s/m_t^2) + \mathcal{O}(m_t^2)$.

2.3.2 Large mass expansion

The large mass limit $m_t \rightarrow \infty$ (or $|s| \rightarrow 0$) of the amplitude eq. (3.8) can easily be obtained as an all order expression in the dimensional regulator ε , by employing the method of regions. It therefore can be used as a non-trivial check of the higher order terms of M_{NLO}^0 in eq. (2.3).

The LO-amplitude for the limit $m_t \gg s$ is obtained by expanding the Feynman parametrization using the tool **asy.m**. We find the all orders expression

$$\begin{aligned}
\mathcal{M}_{\text{LO}}^{0,m_t \rightarrow \infty} &= \frac{2i}{v^0} \frac{\alpha_s^0 S_\varepsilon \mu^{-2\varepsilon}}{4\pi} \left(\frac{m_t^2}{\mu^2} \right)^{-\varepsilon} C_\varepsilon^{\text{LO}} \\
&= \frac{2i}{v^0} \frac{\alpha_s^0 S_\varepsilon \mu^{-2\varepsilon}}{4\pi} \left(\frac{m_t^2}{\mu^2} \right)^{-\varepsilon} \left(-\frac{1}{3} e^{\gamma_E \varepsilon} \Gamma(\varepsilon + 1) \right).
\end{aligned} \tag{2.25}$$

The NLO amplitude eq. (2.3) in the limit $m_t \rightarrow \infty$ factorizes as

$$\mathcal{M}_{\text{NLO}}^{0,m_t \rightarrow \infty} = \frac{2i}{v^0} \left(\frac{\alpha_s^0 S_\varepsilon \mu^{-2\varepsilon}}{4\pi} \right)^2 \left(\left(-\frac{s}{\mu^2} \right)^{-\varepsilon} \left(\frac{m_t^2}{\mu^2} \right)^{-\varepsilon} C_\varepsilon^{\text{LO}} C_\varepsilon^{\text{EFT}} + \left(\frac{m_t^2}{\mu^2} \right)^{-2\varepsilon} C_\varepsilon^{\text{hh}} \right), \tag{2.26}$$

where we separate the terms that correspond to different regions (in the sense of expansions by regions). The first term in (2.26) corresponds to the hard soft region $m_t \sim k_1 \gg k_2, p_1, p_2$ where k_1 denotes the top-loop momentum and the p_i are external momenta. $C_\varepsilon^{\text{LO}}$ is given in (2.25) and

$$C_\varepsilon^{\text{EFT}} = -\frac{6e^{\gamma_E \varepsilon} (\varepsilon^3 + 2\varepsilon^2 - 3\varepsilon + 1) \Gamma(1 - \varepsilon)^2 \Gamma(\varepsilon + 1)}{(1 - 2\varepsilon)(1 - \varepsilon)\varepsilon^2 \Gamma(1 - 2\varepsilon)} \tag{2.27}$$

is the one-loop contribution to $gg \rightarrow H$ in the heavy top EFT (see e.g. eq (3.5) in [49]). The second term in (2.26)

$$C_\varepsilon^{\text{hh}} = \frac{e^{2\gamma_E \varepsilon} \varepsilon^2 (52\varepsilon^3 + 20\varepsilon^2 - 15\varepsilon + 54) \Gamma(\varepsilon)^2}{9(4\varepsilon^3 - 13\varepsilon - 6)} \quad (2.28)$$

corresponds to the double hard region $m_t \sim k_1 \sim k_2 \gg p_1, p_2$. These all-order results in the dimensional regulator ε were obtained by expanding the momentum space representation of the loop integrals in each region and directly integrating the result.

On the other hand, we can expand our results for the bare amplitudes (2.1) in terms of harmonic polylogarithms in the limit $m_t \rightarrow \infty$ with the help of HYPERINT and POLYLOGTOOLS. Including the normalization we have

$$\begin{aligned} \mathcal{M}_{\text{LO}}^{0, m_t \rightarrow \infty} &= \frac{2i}{v^0} \frac{\alpha_s^0 S_\varepsilon \mu^{-2\varepsilon}}{4\pi} \left(-\frac{s}{\mu^2}\right)^{-\varepsilon} M_{\text{LO}}^{0, m_t \rightarrow \infty} \\ &= \frac{2i}{v^0} \frac{\alpha_s^0 S_\varepsilon \mu^{-2\varepsilon}}{4\pi} \left(-\frac{1}{3}\right) \left(1 - \varepsilon \log\left(\frac{m_t^2}{\mu^2}\right) + \frac{1}{12} \varepsilon^2 \left[6 \log^2\left(\frac{m_t^2}{\mu^2}\right) + \pi^2\right] \right. \\ &\quad \left. + \frac{1}{12} \varepsilon^3 \left[-2 \log^3\left(\frac{m_t^2}{\mu^2}\right) - \pi^2 \log\left(\frac{m_t^2}{\mu^2}\right) - 4\zeta_3\right] \right. \\ &\quad \left. + \frac{1}{480} \varepsilon^4 \left[20 \log\left(\frac{m_t^2}{\mu^2}\right) \left(\log^3\left(\frac{m_t^2}{\mu^2}\right) + \pi^2 \log\left(\frac{m_t^2}{\mu^2}\right) + 8\zeta_3\right) + 3\pi^4\right] \right. \\ &\quad \left. + \mathcal{O}(\varepsilon^5)\right). \end{aligned} \quad (2.29)$$

The result agrees with (2.25) expanded to $\mathcal{O}(\varepsilon^4)$, which is an important check of our computation.

For the two-loop pieces we find by directly expanding the result eq. (2.3) in terms of harmonic polylogarithms in the large top-mass limit

$$\begin{aligned} \mathcal{M}_{\text{NLO}}^{0, m_t \rightarrow \infty} &= \frac{2i}{v^0} \left(\frac{\alpha_s^0 S_\varepsilon \mu^{-2\varepsilon}}{4\pi}\right)^2 \left(-\frac{s}{\mu^2}\right)^{-2\varepsilon} M_{\text{NLO}}^{0, m_t \rightarrow \infty} \\ &= \frac{2i}{v^0} \left(\frac{\alpha_s^0 S_\varepsilon \mu^{-2\varepsilon}}{4\pi}\right)^2 \\ &\quad \times \left(\frac{2}{\varepsilon^2} - \frac{2}{\varepsilon} \left[\log\left(\frac{m_t^2}{\mu^2}\right) + \log\left(-\frac{s}{\mu^2}\right)\right] \right. \\ &\quad \left. + 2 \left[\log\left(-\frac{s}{\mu^2}\right) \log\left(\frac{m_t^2}{\mu^2}\right) + \log^2\left(\frac{m_t^2}{\mu^2}\right) + \log^2\left(-\frac{s}{\mu^2}\right) - 1\right] \right. \\ &\quad \left. + \varepsilon \left[-\log\left(-\frac{s}{\mu^2}\right) \log^2\left(\frac{m_t^2}{\mu^2}\right) - \left(\log^2\left(-\frac{s}{\mu^2}\right) - 2\right) \log\left(\frac{m_t^2}{\mu^2}\right) \right. \right. \\ &\quad \left. \left. - \frac{1}{3} \log^3\left(\frac{m_t^2}{\mu^2}\right) - \frac{1}{3} \log^3\left(-\frac{s}{\mu^2}\right) + \frac{8}{9}(5 - 6\zeta_3)\right] \right. \\ &\quad \left. + \varepsilon^2 \left[\frac{1}{3} \log\left(-\frac{s}{\mu^2}\right) \log^3\left(\frac{m_t^2}{\mu^2}\right) + \frac{1}{2} \left(\log^2\left(-\frac{s}{\mu^2}\right) - 4\right) \log^2\left(\frac{m_t^2}{\mu^2}\right) \right] \right) \end{aligned}$$

$$\begin{aligned}
& + \frac{1}{9} \log \left(\frac{m_t^2}{\mu^2} \right) \left(3 \log^3 \left(-\frac{s}{\mu^2} \right) + 48\zeta_3 - 62 \right) + \frac{1}{12} \log^4 \left(\frac{m_t^2}{\mu^2} \right) \\
& + \frac{1}{12} \log^4 \left(-\frac{s}{\mu^2} \right) + \frac{2}{3} (8\zeta_3 - 3) \log \left(-\frac{s}{\mu^2} \right) + \frac{1}{30} (10 - 5\pi^2 - 2\pi^4) \Big] \Big)
\end{aligned} \tag{2.30}$$

and in particular

$$\begin{aligned}
-\frac{1}{3} M_{\text{fin}}^{0, m_t \rightarrow \infty} &= 11 + \left[-\frac{\pi^2}{12} \beta_0 + 28 \log(z) + 12\zeta_3 - \frac{40}{3} \right] \varepsilon \\
&+ \left[\beta_0 \left(-\frac{1}{6} \pi^2 \log(z) - \frac{\zeta_3}{3} \right) + \left(24\zeta_3 - \frac{124}{3} \right) \log(z) + 40 \log^2(z) \right. \\
&\quad \left. + \frac{\pi^4}{5} + \frac{7\pi^2}{6} - 1 \right] \varepsilon^2 + \mathcal{O}(\varepsilon^3)
\end{aligned} \tag{2.31}$$

and

$$\begin{aligned}
-\frac{1}{3} M_{\text{fin, scale}}^{0, m_t \rightarrow \infty} &= -\beta_0 + \left[-\frac{1}{2} \beta_0 \log \left(-\frac{s}{\mu^2} \right) - 2\beta_0 \log(z) + 8 \right] \varepsilon \\
&+ \left[-\frac{\pi^2 \beta_0}{12} - \frac{1}{6} \beta_0 \log^2 \left(-\frac{s}{\mu^2} \right) + 4 \log \left(-\frac{s}{\mu^2} \right) \right. \\
&\quad \left. + \log(z) \left(16 - \beta_0 \log \left(-\frac{s}{\mu^2} \right) \right) - 2\beta_0 \log^2(z) \right] \varepsilon^2 + \mathcal{O}(\varepsilon^3) ,
\end{aligned} \tag{2.32}$$

where $\log(z) = \frac{1}{2} \log(-s/m_t^2) + \mathcal{O}(m_t^{-1})$.

The large mass expansion (2.30) is in complete agreement with the all order expression (2.26) expanded up to $\mathcal{O}(\varepsilon^2)$. This provides a non-trivial check of the higher orders of the complete result for M_{NLO}^0 in (2.1).

3 Amplitudes and results for $H \rightarrow b\bar{b}$

3.1 Higgs effective field theory

The Higgs Effective Field Theory (HEFT) is obtained by integrating out the top quark from the Standard Model [50]. In practice, as long as we do not describe electroweak corrections, it is equivalent but much simpler to describe our calculation in the context of QCD coupled

to a singlet scalar H with mass m_H^4 , yielding the following bare Lagrangian for the EFT:

$$\begin{aligned}
\mathcal{L}_{\text{HEFT}} = & -\frac{1}{4}G_{\mu\nu}^B G^{B\mu\nu} + \frac{1}{2}\left(\partial_\mu H^B \partial^\mu H^B - \left(m_H^{\text{HEFT},B}\right)^2 (H^B)^2\right) - V(H^B) \\
& + \sum_{\psi=u,d,c,s} i\bar{\psi}^B \not{D}\psi^B + i\bar{b}^B \left(\not{D} - m_b^{\text{HEFT},B}\right) b^B + \mathcal{L}_{\text{gf}} \\
& - \frac{C_1^B}{4v^B} H^B G_{\mu\nu}^B G^{B\mu\nu} - C_2^B y_b^{\text{HEFT},B} H^B \bar{b}^B b^B \\
& + \sum_{i=3}^6 C_i^B O_i^B,
\end{aligned} \tag{3.1}$$

where $G_{\mu\nu}$ is the gluon field strength tensor for the gluon field G_μ . H is the scalar Higgs field with mass m_H . The four light quarks $\psi \in \{u, d, c, s\}$ and the massive quark b are labelled by the usual SM flavor symbols. The b -quark mass and Yukawa coupling are denoted by m_b^{HEFT} and $y_b^{\text{HEFT},B} C_2$ where $y_b^{\text{HEFT},B} = m_b^{\text{HEFT},B}/v^B$ and C_2 is the HEFT correction factor to the bottom Yukawa: when matching the HEFT to the SM $C_2 = 1 + \mathcal{O}(1/m_t)$.

We leave unspecified the details of the gauge-fixing and ghost Lagrangian of the gauge interaction \mathcal{L}_{gf} . The couplings mediated by C_1 and $C_{3,\dots,6}$ correspond to the next to leading power terms in the expansion of the exact Lagrangian in powers of the top mass, which we only show explicitly for C_1 since the other operators do not contribute to on shell amplitudes [50]. Note that due to the absence of a Higgs mechanism in our UV-complete theory, the top quark mass and Yukawa are not necessarily related so that we can consistently distinguish power counting in y_t and m_t . Consequently, C_1 is labelled as next-to-leading power despite being non-decoupling when matched to the full SM, where $C_1 \propto y_t/m_t$.

We provide our results expressed in terms of HEFT parameters exclusively, leaving the matching to SM parameters to future applications. As a result, and for the sake of readability, we will drop explicit HEFT labels in the couplings and masses in the rest of this section, as we never refer to SM parameters.

3.2 Notation for bare amplitudes

The bare amplitude $\mathcal{A}_{H \rightarrow b\bar{b}}^B$ of the process $H \rightarrow b(p_1)\bar{b}(p_2)$ can be written to all orders as

$$\mathcal{A}_{H \rightarrow b\bar{b}}^B = \delta_{ij} \bar{u}_\sigma(p_1) \mathcal{M}^B(p_1, p_2) v_{\sigma'}(p_2), \tag{3.2}$$

where \mathcal{M}^B is a Dirac matrix and i, j are color indices of the fundamental representation of $SU(3)$. The external kinematics obey

$$p_1^2 = p_2^2 = m_b^2, \quad (p_1 + p_2)^2 = s, \tag{3.3}$$

⁴The left-handed top quark is part of a $SU(2)$ doublet together with the b quark so integrating out breaks manifest gauge invariance.

where both m_b^2 and s are finite numbers (*i.e.* the p_i^2 are not the bare masses). \mathcal{M}^B can be decomposed as⁵

$$\mathcal{M}^B(p_1, p_2) = \text{Id } M_0^B + (\not{p}_1 - m_b)M_1^B + (\not{p}_2 + m_b)M_2^B + (\not{p}_1 - m_b)(\not{p}_2 + m_b)M_{12}^B, \quad (3.4)$$

where the M_i^B are scalars and $\mathcal{M}^B(p_1, p_2)$ is obtained by computing the Feynman diagrams for $H \rightarrow b\bar{b}$, amputating the external spinors at the integrand level. Contracting with the external spinors, the Dirac equation imposes $(\not{p}_2 + m_b)v = \bar{u}(\not{p}_1 - m_b) = 0$ so that only M_0^B contributes to the physical amplitude. We can easily extract M_0^B by observing that

$$\sum_{\sigma\sigma'} \bar{u}_\sigma(p_1) \mathcal{M}^B(p_1, p_2) v_{\sigma'}(p_2) \times \bar{v}_{\sigma'}(p_2) u_\sigma(p_1) \quad (3.5)$$

$$= \text{Tr}((\not{p}_1 + m_b) \mathcal{M}^B (\not{p}_2 - m_b)) \quad (3.6)$$

$$= 4(p_1 \cdot p_2 - m_b^2) M_0^B, \quad (3.7)$$

and we will therefore restrict further discussions to the scalar quantity M_0^B , which is obtained with the techniques discussed in section 2.1. We furthermore define the following decomposition

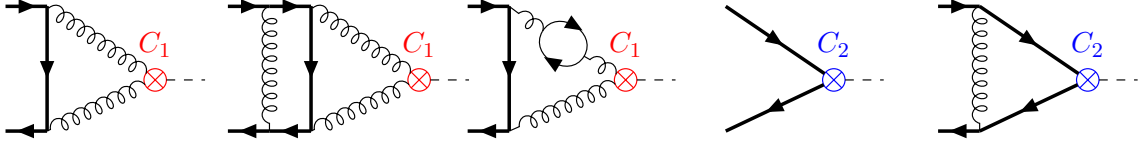


Figure 1: Sample diagrams contributing to $M_{yt,1}^B$, $M_{yt,2}^B$, $M_{yt,lf,2}^B$, $M_{yb,0}^B$ and $M_{yb,1}^B$ in eq. (3.8). Thick directed lines denote massive quarks and thin ones massless quarks.

tion of the amplitude

$$\begin{aligned} M_0^B &= \frac{\alpha_s^B S_\varepsilon \mu^{-2\varepsilon}}{4\pi} \left(-\frac{s}{\mu^2} \right)^{-\varepsilon} \\ &\times \frac{C_1^B}{v^B} \left(M_{yt,1}^B + \frac{\alpha_s^B S_\varepsilon \mu^{-2\varepsilon}}{4\pi} \left(-\frac{s}{\mu^2} \right)^{-\varepsilon} (M_{yt,2}^B + (N_f - 1)M_{yt,lf,2}^B) + \mathcal{O}((\alpha_s^B)^2) \right) \\ &+ y_b^B C_2^B \left(M_{yb,0}^B + \frac{\alpha_s^B S_\varepsilon \mu^{-2\varepsilon}}{4\pi} \left(-\frac{s}{\mu^2} \right)^{-\varepsilon} M_{yb,1}^B + \mathcal{O}((\alpha_s^B)^2) \right), \end{aligned} \quad (3.8)$$

according to the bare coupling structure of the interactions, where

$$S_\varepsilon = (4\pi)^\varepsilon \exp(-\varepsilon \gamma_E). \quad (3.9)$$

In fig. 1 we show sample diagrams contributing to the amplitudes $M_{yt,1}^B$, $M_{yt,2}^B$, $M_{yt,lf,2}^B$, $M_{yb,0}^B$ and $M_{yb,1}^B$ in eq. (3.8). Only $M_{yt,lf,2}^B$ contains contributions from the four light-quarks.

⁵See section A

At face value, computing M_0^B is impractical as there are two different mass parameters for external and internal bottom quarks. We will avoid this issue by renormalizing the bottom quark mass at the Lagrangian level, yielding both a propagator with the renormalized mass and a counter-propagator with the mass counterterm. Note that this has no practical impact on the highest order amplitudes $M_{yt,2}^B$, $M_{yt,lf,2}^B$ and $M_{yb,1}^B$ as any change in the mass yields corrections of higher, neglected order in α_s . Furthermore, $M_{yb,0}^B$ features no bottom-quark propagator, so that only $M_{yt,1}^B$ is affected by the procedure. This effect is also very easy to track since $M_{yt,1}^B$ is generated by a single Feynman diagram with a single bottom quark propagator: the effect of mass renormalization in a scheme where $m_b^B = m_b + \delta m$ is summarized in diagrammatic form as follows

$$\begin{aligned}
M_{yt,1}^B(m_b^B, m_b) &= M_{yt,1}^B(m_b, m_b) + \delta m \times M_{yt,1}^{\text{UV},m}(m_b) \\
\text{Diagram 1} &= \text{Diagram 2} + \delta m \times \text{Diagram 3}
\end{aligned} \tag{3.10}$$

where

$$M_{y_t,1}^{\text{UV},m} = \frac{\partial}{\partial m_b^B} M_{y_t,1}^B(m_b^B, m_b) \Big|_{m_b^B=m_b} \quad (3.11)$$

is generated diagrammatically by replacing the bottom quark propagator by its derivative, which we indicated with a red cross in eq. (3.10), *i.e*

$$\text{---}\blacktriangleright\text{---} = \frac{\partial}{\partial m_b^B} \frac{i\delta_{ij}}{\not{k} - m_b^B} \bigg|_{m_b^B = m_b} = \frac{i\delta_{ik}}{\not{k} - m_b} (-im_b) \frac{i\delta_{kj}}{\not{k} - m_b}. \quad (3.12)$$

We leave the discussion of the renormalization of the mass and the precise definition of δm for the next section. In this section, we instead focus on defining the bare amplitudes in terms of simple components.

We separate the mass-renormalized amplitude $M_{y,1}^B(m_b, m_b)$ according to

$$M_{y_{t,1}}^B(m_b, m_b) = \hat{M}_{y_{t,1}} = M_0^{\text{UV}} + M_{y_{t,1}}^{\text{fin}}, \quad (3.13)$$

and $M_{y_t, 2}^B$ as

$$M_{y_t,2}^B + (N_f - 1)M_{y_t,1f,2}^B = M_1^{\text{UV}} + M_2^{\text{UV}} + M_3^{\text{UV}} + M_{m_b}^{\text{UV}} + M^{\text{IR}} + M_{y_t,2}^{\text{fin.}}, \quad (3.14)$$

such that the poles are separated by IR- and UV-origin respectively. The UV-divergent contribution of the one-loop amplitude reads

$$M_0^{\text{UV}} = - \left(-\frac{s}{\mu^2} \right)^\varepsilon \left(\frac{3m_b C_F}{\varepsilon} \right) M_{y_b,0}^B. \quad (3.15)$$

The two-loop UV-poles are separated according to

$$M_1^{\text{UV}} = - \left(-\frac{s}{\mu^2} \right)^{2\varepsilon} \left[\frac{3m_b C_F}{\varepsilon} \left(-\frac{C_F}{\varepsilon} \right) + \frac{3m_b C_F}{\varepsilon} \left(-\frac{3C_F}{\varepsilon} \right) + C_F \left(\frac{m_b}{\varepsilon^2} (2N_f - 11N_c) + \frac{m_b}{\varepsilon} \frac{(-20N_c N_f + 203N_c^2 - 9)}{12N_c} \right) \right] M_{y_b,0}^B, \quad (3.16)$$

$$M_2^{\text{UV}} = - \left(-\frac{s}{\mu^2} \right)^{\varepsilon} \left(\frac{3m_b C_F}{\varepsilon} \right) M_{y_b,1}^B, \quad (3.17)$$

$$M_3^{\text{UV}} = - \left(-\frac{s}{\mu^2} \right)^{\varepsilon} \left(-\frac{\beta_0}{\varepsilon} - \frac{C_F}{\varepsilon} - \frac{\beta_0}{\varepsilon} \right) \hat{M}_{y_t,1}^B, \quad (3.18)$$

$$M_{m_b}^{\text{UV}} = - \left(-\frac{s}{\mu^2} \right)^{\varepsilon} \left(-\frac{3C_F}{\varepsilon} \right) M_{y_t,1}^{\text{UV},m}, \quad (3.19)$$

where

$$\beta_0 = \frac{11N_c}{3} - \frac{2N_f}{3}, \quad N_f = 5 \quad \text{and} \quad C_F = (N_c^2 - 1)/(2N_c). \quad (3.20)$$

The IR-divergences can be described using the factorization of next-to-leading order amplitudes with massive external colored particles [44]⁶ as

$$M^{\text{IR}} = \left(-\frac{s}{\mu^2} \right)^{\varepsilon} \mathcal{I}_1 M_{y_t,1}^{\text{fin.}} = \left(-\frac{s}{\mu^2} \right)^{\varepsilon} \left(-2C_F \frac{e^{\varepsilon\gamma_E}}{\Gamma(1-\varepsilon)} \left(\frac{\mu^2}{|s-2m_b^2|} \right)^{\varepsilon} V_{qq} \right) M_{y_t,1}^{\text{fin.}} \quad (3.21)$$

with

$$V_{qq} = \frac{1}{6} \left(-3 \log^2 \left(\frac{x}{x^2+1} \right) - \pi^2 \right) - \frac{(x^2+1) \log(x)}{(x^2-1)\varepsilon} \quad (3.22)$$

where

$$x = \frac{\sqrt{4m_b^2 - s} - \sqrt{-s}}{\sqrt{4m_b^2 - s} + \sqrt{-s}} \quad (3.23)$$

In the region where $s < 0$, or equivalently $0 < x < 1$. We discuss the analytic continuation to the physical region $s > 0$ in section 4.

3.3 Renormalization and IR-subtraction

The renormalized amplitude of the process $H \rightarrow b\bar{b}$ reads

$$\mathcal{A}_{H \rightarrow b\bar{b}}(\alpha_s, m_b, C_1, C_2) = \delta_{ij} \bar{u}_\sigma(p_1) \mathcal{M} v_{\sigma'}(p_2) = Z_b \mathcal{A}_{H \rightarrow b\bar{b}}^B(\alpha_s^B, m_b^B, m_b, C_1^B, C_2^B), \quad (3.24)$$

⁶As opposed to [44] we perform the wave-function renormalization in $\overline{\text{MS}}$ (see section 3.3) instead of the on-shell scheme and adjust the \mathcal{I}_1 operator accordingly.

where the superscript B denotes bare quantities, Z_b is the wave-function renormalization function of the massive b -quarks and μ the renormalization scale. The bare and the renormalized parameters are related by

$$\alpha_s^B = \frac{\mu^{2\varepsilon}}{S_\varepsilon} Z_{\alpha_s} \alpha_s, \quad m_b^B = m_b + \delta m = Z_m m_b, \quad (3.25)$$

$$v^B = \mu^{-\varepsilon} v, \quad \begin{pmatrix} C_1^B \\ C_2^B \end{pmatrix} = \begin{pmatrix} Z_{11} & 0 \\ Z_{21} & 0 \end{pmatrix} \begin{pmatrix} C_1 \\ C_2 \end{pmatrix}, \quad (3.26)$$

where the renormalization constants Z_X are parametrized as

$$Z_X = 1 + \frac{\alpha_s}{4\pi} \delta Z_X^{(1)} + \frac{\alpha_s^2}{(4\pi)^2} \delta Z_X^{(2)} + \mathcal{O}(\alpha_s^3). \quad (3.27)$$

The y_b -renormalization is completely determined by the mass renormalization. The part of the renormalized amplitude that is proportional to C_1 reads

$$\begin{aligned} \mathcal{M}_{H \rightarrow b\bar{b}} \Big|_{C_1} = & \frac{1}{2(s - 4m_b^2)} \frac{C_1}{v} \frac{\alpha_s}{4\pi} \left(-\frac{s}{\mu^2} \right)^{-\varepsilon} \times \left[M_{y_t,1} + \left(-\frac{s}{\mu^2} \right)^\varepsilon \delta Z_{21}^{(1)} M_{y_b,0} \right. \\ & + \frac{\alpha_s}{4\pi} \left(-\frac{s}{\mu^2} \right)^{-\varepsilon} \left(\left(-\frac{s}{\mu^2} \right)^{2\varepsilon} \left[\delta Z_{21}^{(1)} \delta Z_b^{(1)} + \delta Z_{21}^{(1)} \delta Z_m^{(1)} + \delta Z_{21}^{(2)} \right] M_{y_b,0} \right. \\ & + \left(-\frac{s}{\mu^2} \right)^\varepsilon \delta Z_{21}^{(1)} M_{y_b,1} + \left(-\frac{s}{\mu^2} \right)^\varepsilon \left(\delta Z_{\alpha_s}^{(1)} + \delta Z_b^{(1)} + \delta Z_{11}^{(1)} \right) M_{y_t,1} \\ & \left. \left. + \left(-\frac{s}{\mu^2} \right)^\varepsilon \delta Z_m^{(1)} M_{y_t,1}^{\text{UV},m} + M_{y_t,2} + (N_f - 1) M_{y_t,\text{lf},2} \right] \right], \quad (3.28) \end{aligned}$$

where the scalar quantities $M_X(m_b)$ are defined in the previous section. We renormalize our amplitude in $\overline{\text{MS}}$ with the relevant renormalization constants [51–53]

$$Z_b = 1 + \frac{\alpha_s}{4\pi} \left(-\frac{C_F}{\varepsilon} \right) + \mathcal{O}(\alpha_s^2) \quad (3.29)$$

$$Z_{\alpha_s} = 1 + \frac{\alpha_s}{4\pi} \left(\frac{2N_f - 11N_c}{3\varepsilon} \right) + \mathcal{O}(\alpha_s^2) \quad (3.30)$$

$$\begin{aligned} Z_m = & 1 + \frac{\alpha_s}{4\pi} \left(-\frac{3C_F}{\varepsilon} \right) + \frac{\alpha_s^2}{(4\pi)^2} C_F \left(\frac{1}{\varepsilon^2} \left(\frac{31N_c}{4} - \frac{9}{4N_c} - N_f \right) \right. \\ & \left. + \frac{1}{\varepsilon} \left(\frac{-203N_c}{24} + \frac{3}{8N_c} + \frac{10N_f}{12} \right) \right) + \mathcal{O}(\alpha_s^3) \quad (3.31) \end{aligned}$$

$$Z_{11} = 1 + \frac{\alpha_s}{4\pi} \frac{4\pi \partial \log(Z_{\alpha_s})}{\partial \alpha_s} \quad (3.32)$$

$$Z_{21} = -\frac{\alpha_s}{4\pi} \frac{4\pi \partial \log(Z_m)}{\partial \alpha_s}. \quad (3.33)$$

Comparing with eq. (3.13) and eq. (3.14) yields the $\overline{\text{MS}}$ renormalized amplitude

$$\mathcal{M}_{H \rightarrow b\bar{b}} \Big|_{C_1}^{\overline{\text{MS}}} = \frac{1}{2(s - 4m_b^2)} \frac{C_1}{v} \frac{\alpha_s}{4\pi} \left(-\frac{s}{\mu^2} \right)^{-\varepsilon} \quad (3.34)$$

$$\times \left[M_{y_t,1}^{\text{fin}} + \frac{\alpha_s}{4\pi} \left(-\frac{s}{\mu^2} \right)^{-\varepsilon} \left(M_{y_t,2}^{\text{fin}} + M^{\text{IR}} \right) \right],$$

We provide all contributions to the bare amplitudes $M_{y_x,n}^0$ as well as the renormalized and IR-subtracted amplitudes $M_{y_t,(1,2)}^{\text{fin}}$ in the ancillary material, such that results for a different choice of a renormalization scheme can be easily obtained (see section 2.2). We furthermore provide all necessary master integrals for this process up to weight 6, such that higher orders in the dimensional regulator are easily accessible for future computations.

3.4 Small mass expansion

In the limit where $m_b^2 \ll |(p_1 \cdot p_2)|$ the renormalized and IR-subtracted amplitudes have the expansion

$$M_{y_t,1}^{\text{fin}} \Big|_{m_b^2 \ll |(p_1 \cdot p_2)|} = -sm_b i \left(-2 \log \left(\frac{\mu^2}{m_b^2} \right) + \frac{1}{3} \log^2 \left(\frac{m_b^2}{-s} \right) + \frac{4}{9} (\pi^2 - 6) \right) + \mathcal{O}(m_b^2) \quad (3.35)$$

and

$$\begin{aligned} M_{y_t,2}^{\text{fin}} \Big|_{m_b^2 \ll |(p_1 \cdot p_2)|} = & -sm_b i \left(\log \left(\frac{\mu^2}{m_b^2} \right) \left(\frac{62}{9} \log^2 \left(\frac{m_b^2}{-s} \right) + \frac{8}{3} \log \left(\frac{m_b^2}{-s} \right) \right. \right. \\ & + \frac{2}{27} (124\pi^2 - 1575) \Big) - 26 \log^2 \left(\frac{\mu^2}{m_b^2} \right) - \frac{5}{54} \log^4 \left(\frac{m_b^2}{-s} \right) \\ & + \frac{68}{27} \log^3 \left(\frac{m_b^2}{-s} \right) + \frac{1}{27} (533 + 2\pi^2) \log^2 \left(\frac{m_b^2}{-s} \right) \\ & + \frac{8}{27} (3\zeta_3 + 11\pi^2) \log \left(\frac{m_b^2}{-s} \right) \\ & \left. + \frac{1}{810} (38520\zeta_3 - 134895 + 20980\pi^2 - 554\pi^4) \right) + \mathcal{O}(m_b^2) , \quad (3.36) \end{aligned}$$

with $s \approx 2(p_1 \cdot p_2)$. We found these results to agree with [54].

4 Analytic continuation for $gg \rightarrow H$ and $H \rightarrow b\bar{b}$

Our results are provided in the Euclidean regime $s < 0$ and we discuss in the following how they can analytically be continued to the physical regime. The amplitude $gg \rightarrow H$ has the production threshold at $s = 4m_t^2$ and the pseudo threshold $s = 0$. A parametrization of the amplitude in terms of the “natural” scaleless ratio s/m_t^2 will yield undesirable roots of the form

$$\sqrt{-\frac{s}{m_t^2}} \sqrt{4 - \frac{s}{m_t^2}} . \quad (4.1)$$

The same happens for $H \rightarrow b\bar{b}$, where the scaleless variable s/m_b^2 gives rise to the same roots. To make discussion valid for both amplitudes under consideration, we introduce the scaleless ratio

$$y = \frac{s}{m_q^2} = \begin{cases} \frac{(p_1+p_2)^2}{m_t^2} ; & g(p_1)g(p_2) \rightarrow H ; & p_i^2 = 0 \\ \frac{(p_1+p_2)^2}{m_b^2} ; & H \rightarrow b(p_1)\bar{b}(p_2) ; & p_i^2 = m_b^2 \end{cases} . \quad (4.2)$$

To rationalize the roots we work with the scaleless complex variable x defined by

$$x = \lim_{\eta \downarrow 0^+} \frac{\sqrt{4 - (y + i\eta)} - \sqrt{-(y + i\eta)}}{\sqrt{4 - (y + i\eta)} + \sqrt{-(y + i\eta)}} \quad (4.3)$$

with

$$y = \frac{-(1-x)^2}{x} \quad (4.4)$$

and $0 < |x| < 1$. Here Feynman's prescription is denoted by $+i\eta$, implicitly defining the branch on which to evaluate the roots in the definition of x eq. (4.3). More explicitly we have

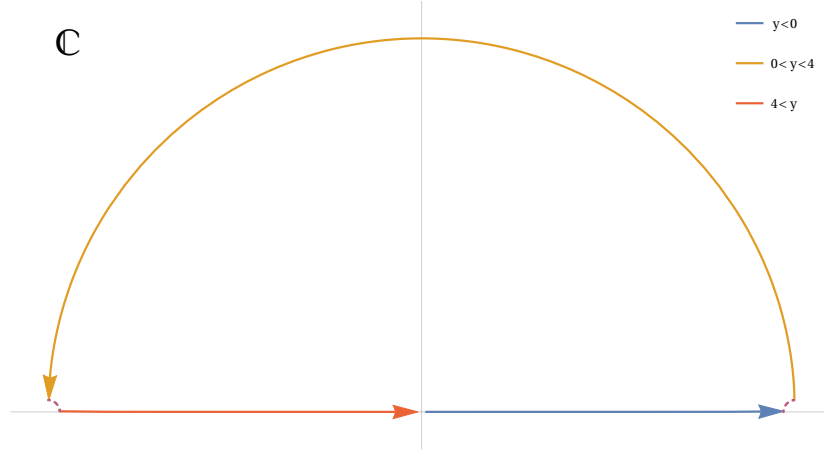


Figure 2: Representation of the complex variable $x = \frac{\sqrt{4-(y+i\eta)} - \sqrt{-(y+i\eta)}}{\sqrt{4-(y+i\eta)} + \sqrt{-(y+i\eta)}}$ for all kinematic regions. Feynman's prescription is denoted by the explicit $+i\eta$.

$$x + i \lim_{\eta \downarrow 0^+} \eta = \begin{cases} \frac{\sqrt{4-y} - \sqrt{-y}}{\sqrt{4-y} + \sqrt{-y}}; & y < 0 \\ -e^{i(\phi-\pi)}; & \phi = \arctan\left(\frac{\sqrt{(4-y)y}}{2-y}\right); & 0 < y < 2 \\ -e^{i\phi}; & \phi = \arctan\left(\frac{\sqrt{(4-y)y}}{2-y}\right); & 2 < y < 4 \\ \frac{\sqrt{y-4} - \sqrt{y}}{\sqrt{y-4} + \sqrt{y}}; & 4 < y \end{cases} . \quad (4.5)$$

The last line indicates that above threshold ($s > 4m_q^2$) where $-1 < x < 0$, x has to be evaluated by approaching the negative real axis from the upper half plane. The variable x is shown in fig. 2.

The complete result of for $gg \rightarrow H$ at NLO as well as $H \rightarrow b\bar{b}$ can be expressed in terms of harmonic polylogarithms [55] with argument x eq. (4.3). A harmonic polylogarithm of weight n is defined as the iterated integral

$$H(a_n, a_{n-1}, \dots, a_1; x) = \int_0^x H(a_{n-1}, \dots, a_1; t) f(a_n, t) dt , \quad (4.6)$$

where $a_i \in \{1, 0, -1\}$ and

$$f(1, t) = \frac{1}{1-t} , \quad f(0, t) = \frac{1}{t} \quad \text{and} \quad f(-1, t) = \frac{1}{1+t} . \quad (4.7)$$

For the case of all a_n, \dots, a_1 being zero we define

$$H(\underbrace{0, 0, \dots, 0}_{n\text{-times}}; x) = \frac{1}{n!} \log^n(x) . \quad (4.8)$$

Harmonic polylogarithms form a shuffle algebra [55] and have a branch point at $x = 0$ if and only if $a_1 = 0$. If $a_1 = 0$ one can use the shuffle algebra and rewrite the HPL as a linear combination of products of HPLs such that every HPL of weight $j \leq n$ appearing in this linear combination which has $a_1 = 0$ has also $a_k = 0$ for all $k = 2, \dots, j$, *i.e.* all discontinuities around $x = 0$ can be described by a polynomial in $\log(x)$. This method of explicitly extracting the logarithmic factors is implemented in several publicly available codes [48, 56–58], among which we chose POLYLOGTOOLS to perform this task. Once the logarithms are extracted explicitly, as in the provided ancillary material, the complete analytic continuation to the regime $s > 4m_q^2$ is obtained by performing the limit

$$\lim_{\eta \downarrow 0^+} \log(x + i\eta) = \log(-x) + i\pi . \quad (4.9)$$

All other regimes have no subtleties and can be evaluated by using the explicit prescription in the right-hand side of eq. (4.5).

5 Computation of master integrals

We define a generic l -loop integral depending on the kinematic invariant s and the mass $m_q > 0$ as

$$I_{\nu_1, \dots, \nu_n} = \left(m_q^{2\varepsilon} \frac{e^{\gamma_E \varepsilon}}{i\pi^{d/2}} \right)^l \int d^d k_1 \dots d^d k_l \frac{1}{D_1^{\nu_1} \dots D_n^{\nu_n}} , \quad (5.1)$$

where the D 's denote the propagators, the $\nu_i \in \mathbb{Z}$ their respective powers and the normalization is chosen to render the integrals scaleless.

We employ two methods for analytically computing loop integrals.

The first is based on writing the integral in terms of Feynman parameters and attempting a direct integration. Powerful tools like programs HYPERINT and POLYLOGTOOLS are dedicated towards performing these parametric integrals.

The second technique is based on deriving a closed system of differential equations [59, 60]. Instead of attempting a direct integration of the integrals, one tries solving a corresponding system of coupled first order differential equations obtained by taking derivatives with respect to all external and internal scales s_i . In [61] it was conjectured that for a large class of Feynman integrals a particular basis choice of MIs can be found, such that the dependence of the dimensional regulator factors out completely. For such a *canonical* basis the total differential takes the particular simple form

$$d\vec{I}^n = dA \cdot \vec{I}^{n-1} , \quad (5.2)$$

where \vec{I}^n denotes n th Laurent coefficient of the integrals and the matrix A depends on the external and internal scales s_i only. A formal, general solution of the system of differential equations eq. (5.2) for every Laurent-coefficient in the ε -expansion of the canonical integrals can be written down in terms of Chen iterated integrals [62] directly. If the entries of the matrix A are \mathbb{Q} -linear combinations of logarithms one can often find a solution in terms of multiple polylogarithms [63] defined for $a_k \neq 0$ by the iterated integral

$$G(a_1, a_2, \dots, a_k; z) = \int_0^z \left(\int_0^{x_1} \left(\dots \left(\int_0^{x_{k-1}} \frac{dx_k}{x_k - a_k} \right) \dots \right) \frac{dx_2}{x_2 - a_2} \right) \frac{dx_1}{x_1 - a_1} . \quad (5.3)$$

For the special case where all $a_i \in \{1, 0, -1\}$ they reduce to harmonic polylogarithms defined in eq. (4.6), which appear in the amplitudes under consideration.

5.1 Master integrals for M_{LO}^0 in $gg \rightarrow H$

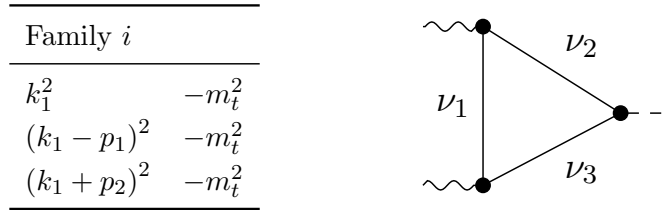


Figure 3: Definition of the completed family necessary to parametrize all diagrams in M_{LO}^0 . The loop momentum is denoted by k_1 while p_1 and p_2 are the momenta of the incoming gluons and m_t is the quark mass. In the diagram the dashed line corresponds to the Higgs, wavy lines denote massless and continuous straight lines massive propagators.

The one-loop contribution M_{LO}^0 in $\mathcal{A}_{gg \rightarrow H}^0$ eq. (2.1) gives rise to one integral family shown in fig. 3 which has three MIs. We choose the following basis

$$f_i^1 = \varepsilon i_{0,0,2} , \quad f_i^2 = \varepsilon \frac{(x^2 - 1)m_t^2}{x} i_{0,1,2} , \quad f_i^3 = -\varepsilon^2 \frac{(x - 1)^2 m_t^2}{x} i_{1,1,1} \quad (5.4)$$

and we report all necessary coefficients to compute $\mathcal{A}_{gg \rightarrow H}^0$ eq. (2.1) to $\mathcal{O}(\varepsilon^2)$ in the ancillary files. The computation of the master integrals was done by performing the Feynman parameter integral with the help of the program HYPERINT.

For the computation of $M_{uv,m}^0$ eq. (2.5), corresponding to the mass renormalization, we need the mass derivatives of the one-loop MIs. Since we defined a canonical basis, they take the particular simple form:

$$\frac{\partial}{\partial m_t^2} f_i^{1,n} = 0 \quad (5.5)$$

$$\frac{\partial}{\partial m_t^2} f_i^{2,n} = \frac{(x-1)^2}{(x+1)^2 m_t^2} f_i^{2,n-1} + \frac{(x-1)}{(x+1) m_t^2} f_i^{1,n-1} \quad (5.6)$$

$$\frac{\partial}{\partial m_t^2} f_i^{3,n} = \frac{(x-1)}{(x+1) m_t^2} f_i^{2,n-1}, \quad (5.7)$$

where $f_i^{k,n}$ denotes the n th Laurent coefficient of the k th MI.

5.2 Master integrals for M_{NLO}^0 in $gg \rightarrow H$

| Family a | | Family b | | Family c | |
|-----------------------|----------|-----------------------|----------|-----------------------|----------|
| k_1^2 | | k_1^2 | $-m_t^2$ | k_1^2 | $-m_t^2$ |
| $(k_1 - k_2)^2$ | $-m_t^2$ | $(k_1 - k_2)^2$ | | $(k_1 - k_2)^2$ | |
| k_2^2 | $-m_t^2$ | $(k_1 - k_2 - p_1)^2$ | | k_2^2 | $-m_t^2$ |
| $(k_1 + p_1 + p_2)^2$ | | $(k_2 + p_1)^2$ | $-m_t^2$ | $(k_2 + p_2)^2$ | $-m_t^2$ |
| $(k_2 + p_1 + p_2)^2$ | $-m_t^2$ | $(k_1 + p_1 + p_2)^2$ | $-m_t^2$ | $(k_1 + p_1 + p_2)^2$ | $-m_t^2$ |
| $(k_1 + p_1)^2$ | | $(k_2 + p_1 + p_2)^2$ | $-m_t^2$ | $(k_2 + p_1 + p_2)^2$ | $-m_t^2$ |
| $(k_2 + p_1)^2$ | $-m_t^2$ | $(k_1 + p_1)^2$ | $-m_t^2$ | $(k_1 + p_2)^2$ | $-m_t^2$ |

Table 1: Definition of the completed families necessary to parametrize all diagrams in M_{NLO}^0 2.3. The loop momenta are denoted by k_1 and k_2 , p_1 and p_2 are the momenta of the incoming gluons and m_t is the quark mass.

All scalar integrals of the complete two-loop form factor M_{NLO}^0 eq. (2.3) can be written in terms of integrals of the three auxiliary families a , b and c listed in table 1. In order to compute this NLO contribution to $gg \rightarrow H$ with full mass dependence to $\mathcal{O}(\varepsilon^2)$ a total of 18 two-loop master integrals (MIs) have to be computed to higher orders in the dimensional regulator than known in the literature [8, 64–66]. The topologies corresponding to the MIs are depicted in fig. 4, where the dashed line corresponds to the Higgs, wavy lines denote massless and continuous straight lines massive propagators. The ν_i denote the i th propagator and the superscripts A , B , and C denote the corresponding scalar family. As a canonical basis of integrals we chose the set eq. (5.8). The corresponding topologies appear already as a subset

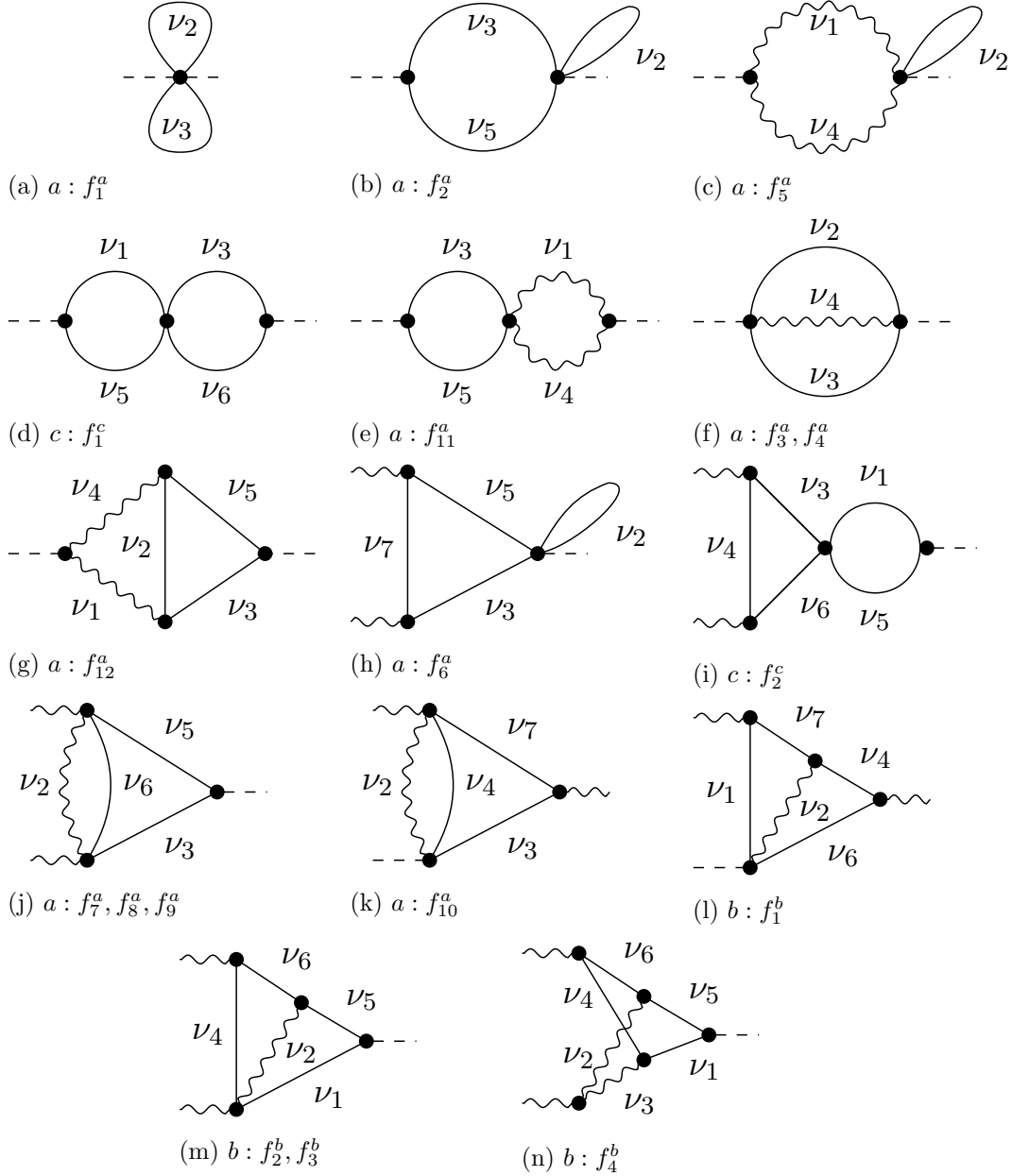


Figure 4: Scalar two-loop topologies contributing to M_{NLO}^0 eq. (2.3). The dashed line corresponds to the Higgs, wavy lines denote massless and continuous straight lines massive propagators. The letters in the captions stand for the corresponding completed family a , b or c while the ν_i denote the relevant propagators. The f_i^j are the canonical MI of the depicted topology. Diagrams are generated with TikZ-Feynman [67].

of integrals in [17] and we deviate from their choice of MIs only slightly.

$$f_1^a = \varepsilon^2 a_{0,2,2,0,0,0,0}$$

$$f_2^a = \frac{m_t^2 (x^2 - 1) \varepsilon^2 a_{0,2,2,0,1,0,0}}{x}$$

$$\begin{aligned}
f_3^a &= -\frac{m_t^2(x-1)^2 \varepsilon^2 a_{0,2,2,1,0,0,0}}{x} \\
f_4^a &= \frac{m_t^2(x^2-1) \varepsilon^2 (2a_{0,2,1,2,0,0,0} + a_{0,2,2,1,0,0,0})}{2x} \\
f_5^a &= -\frac{m_t^2(x-1)^2 \varepsilon^2 a_{1,2,0,2,0,0,0}}{x} & f_6^a &= -\frac{m_t^2(x-1)^2 \varepsilon^3 a_{0,2,1,0,1,0,1}}{x} \\
f_7^a &= -\frac{m_t^2(x-1)^2 \varepsilon^3 a_{0,2,1,0,1,1,0}}{x} & f_8^a &= -\frac{m_t^4(x-1)^2 \varepsilon^2 a_{0,3,1,0,1,1,0}}{x} \\
f_9^a &= -\frac{3m_t^2(x^2-1) \varepsilon^2 (2m_t^2(a_{0,2,2,0,1,1,0} + a_{0,3,1,0,1,1,0}) + 3\varepsilon a_{0,2,1,0,1,1,0})}{2x} \\
f_{10}^a &= -\frac{m_t^2(x-1)^2 \varepsilon^3 a_{0,2,1,1,0,0,1}}{x} & f_{11}^a &= -\frac{m_t^4(x-1)^3(x+1) \varepsilon^2 a_{2,0,2,1,1,0,0}}{x^2} \\
f_{12}^a &= \frac{m_t^2(x-1)^2 \varepsilon^3 (2\varepsilon-1) a_{1,1,1,1,1,0,0}}{x} \\
f_1^b &= -\frac{m_t^2(x-1)^2 \varepsilon^4 b_{1,1,0,1,0,1,1}}{x} & f_2^b &= -\frac{m_t^2(x-1)^2 \varepsilon^4 b_{1,1,0,1,1,1,0}}{x} \\
f_3^b &= -\frac{m_t^4(x-1)^3(x+1) \varepsilon^3 b_{2,1,0,1,1,1,0}}{x^2} & f_4^b &= \frac{m_t^4(x-1)^4 \varepsilon^4 b_{1,1,1,1,1,1,0}}{x^2} \\
f_1^c &= \frac{m_t^4(x^2-1)^2 \varepsilon^2 c_{2,0,2,0,1,1,0}}{x^2} & f_2^c &= -\frac{m_t^4(x-1)^3(x+1) \varepsilon^3 c_{2,0,1,1,1,1,0}}{x^2} \quad (5.8)
\end{aligned}$$

We derive the differential equation using LITERED, [68] perform the necessary IBP-reduction with KIRA and integrate the differential equation order-by-order in ε . As a boundary point we consider the point $x = 1$ corresponding to $s/m_t^2 = 0$. The only non vanishing integrals in this limit are the basis integrals f_1^a and f_5^a

$$f_1^a = e^{2\gamma_E \varepsilon} \varepsilon^2 \Gamma(\varepsilon)^2 \quad \text{and} \quad f_5^a = \frac{e^{2\gamma_E \varepsilon} \varepsilon^3 \left(\frac{x}{(x-1)^2} \right)^\varepsilon \Gamma(-\varepsilon)^2 \Gamma(\varepsilon)^2}{2\Gamma(-2\varepsilon)}. \quad (5.9)$$

We checked our results for the MIs numerically in every kinematic regime against the evaluation with the program FIESTA 4.1. The numeric evaluation of the HPL's is performed using the GiNAC [69, 70]. We have complete agreement within the numerical uncertainties of FIESTA 4.1. All Laurent coefficients for all MIs are provided in the ancillary material.

5.3 One-Loop master integrals in $H \rightarrow b\bar{b}$

The one loop-contribution to $H \rightarrow b\bar{b}$ consist of the two contributions $M_{y_b,1}^B$ and $M_{y_t,1}^B$, which mix under renormalization with the two-loop contribution $M_{y_t,2}^B$. The scalar families contributing to the one-loop amplitudes are defined in tab. 2 and shown in fig. 5. Dashed lines corresponds to the Higgs, wavy lines denote massless and continuous straight lines massive propagators and external lines of mass m_b^2 . As a basis of integrals we make the following choice:

$$f_j^1 = f_k^1 = \varepsilon j_{2,0,0} \quad f_j^2 = m_b^2 j_{1,2,0}$$

| Family j : C_2 contribution | Family k : C_1 contribution |
|---------------------------------|---------------------------------|
| $(k - p_1)^2$ | k^2 |
| $-m_b^2$ | $-m_b^2$ |
| $(k + p_2)^2$ | $(k + p_2)^2$ |
| $-m_b^2$ | |
| k^2 | $(k - p_1)^2$ |

Table 2: Definition of the families necessary to parametrize all diagrams appearing in the one-loop contributions to $H \rightarrow b\bar{b}$. The loop momentum is denoted by k , p_1 and p_2 are the momenta of the incoming quarks and m_b is the quark mass.

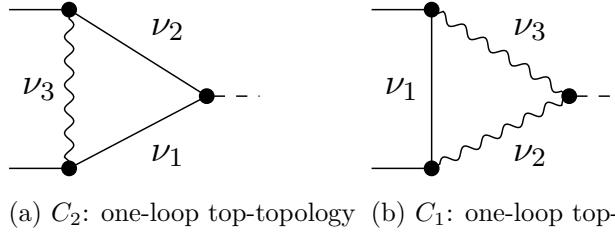


Figure 5: Scalar top-topologies contributing to $M_{yb,1}^B$ and $M_{yt,1}^B$ in eq. (3.8). The dashed line corresponds to the Higgs, wavy lines denote massless and continuous straight lines massive propagators. If a continuous straight line is external it carries momentum $p^2 = m_b^2$. The ν_i denote the relevant propagators.

$$f_k^2 = -\varepsilon \frac{(x-1)^2 m_B^2}{x} k_{0,1,2} \quad f_k^3 = -\varepsilon^2 m_B^2 \frac{(x^2-1)}{x} k_{1,1,1} , \quad (5.10)$$

which we compute with the help of HYPERINT. We provide the Laurent-coefficients up to weight six in the ancillary files.

5.4 Two-Loop master integrals in $H \rightarrow b\bar{b}$

The complete set of scalar integrals of the EFT process $H \rightarrow b\bar{b}$ can be parametrized by the three auxiliary families l, m and n defined in tab. 3. As a set of MIs we take the 25 canonical integrals defined in eq. (5.11), eq. (5.12) and eq. (5.13). The topologies corresponding to the MIs are shown in fig. 6 and fig. 7, where the dashed line corresponds to the Higgs, wavy lines denote massless and continuous straight lines massive propagators and external lines of mass m_b^2 .

$$\begin{aligned} f_1^l &= \varepsilon^2 l_{2,0,0,0,2,0,0} & f_2^l &= \varepsilon^2 l_{0,1,0,2,0,0,2} m_b^2 \\ f_3^l &= -\frac{(x-1)^2 \varepsilon^2 l_{2,0,0,0,0,1,2} m_b^2}{x} \\ f_4^l &= -\frac{(x-1)(x+1) \varepsilon^2 l_{2,0,0,0,0,1,2} m_b^2}{2x} - \frac{(x-1)(x+1) \varepsilon^2 l_{2,0,0,0,0,2,1} m_b^2}{x} \end{aligned}$$

| Family l | | Family m | | Family n | |
|-----------------------|----------|-----------------------|----------|-----------------------------|----------|
| k_1^2 | $-m_b^2$ | k_2^2 | $-m_b^2$ | $(k_1 - p_1)^2$ | $-m_b^2$ |
| $(k_1 + p_1)^2$ | | $(k_1 - p_1)^2$ | $-m_b^2$ | $(k_2 - p_2)^2$ | $-m_b^2$ |
| $(k_1 + p_1 + p_2)^2$ | $-m_b^2$ | $(k_1 - p_1 - p_2)^2$ | | $(k_1 + k_2 - p_1 - p_2)^2$ | |
| k_2^2 | | $(k_2 - p_2)^2$ | | $(k_1 + k_2)^2$ | |
| $(k_2 + p_1)^2$ | $-m_b^2$ | $(k_1 - k_2 - p_1)^2$ | | k_2^2 | |
| $(k_2 + p_1 + p_2)^2$ | | k_1^2 | | k_1^2 | |
| $(k_1 - k_2)^2$ | $-m_b^2$ | $(k_2 + p_1)^2$ | | $(k_1 + k_2 - p_1)^2$ | |

Table 3: Definition of the completed families necessary to parametrize all diagrams appearing in the two-loop contribution to $H \rightarrow b\bar{b}$. The loop momenta are denoted by k_1 and k_2 , p_1 and p_2 are the momenta of the incoming quarks and m_b is the quark mass.

$$\begin{aligned}
f_5^l &= \varepsilon^2 l_{2,0,0,0,2,0,1} m_b^2 & f_6^l &= -\frac{(x-1)^2 \varepsilon^2 l_{2,0,0,2,0,1,0} m_b^2}{x} \\
f_7^l &= -\frac{(x-1)(x+1) \varepsilon^2 l_{2,0,1,0,2,0,0} m_b^2}{x} & f_8^l &= -\frac{(x-1)(x+1) \varepsilon^3 l_{0,1,0,1,0,1,2} m_b^2}{x} \\
f_9^l &= -\frac{(x-1)(x+1) \varepsilon^3 l_{0,2,0,1,0,1,1} m_b^2}{x} \\
f_{10}^l &= \frac{(x-1)^2 \varepsilon^3 l_{0,1,0,1,0,1,2} m_b^2}{x} + \frac{(x-1)^2 \varepsilon^3 l_{0,2,0,1,0,1,1} m_b^2}{2x} - \frac{(x-1)^2 \varepsilon^2 l_{0,1,0,1,0,2,2} m_b^4}{x} \\
f_{11}^l &= -\frac{(x-1)(x+1) \varepsilon^3 l_{2,0,0,0,1,1,1} m_b^2}{x} \\
f_{12}^l &= -\frac{3(x-1)^2(x+1)^2 \varepsilon^3 l_{2,0,0,0,1,1,1} m_b^2}{2x(x^2+1)} - \frac{(x-1)^2(x+1)^2 \varepsilon^2 l_{3,0,0,0,1,1,1} m_b^4}{x(x^2+1)} \\
&\quad + \frac{(x^2+6x+1) \varepsilon^2 l_{2,0,0,0,2,0,1} m_b^2}{2(x^2+1)} \\
f_{13}^l &= -\frac{(x-1)(x+1) \varepsilon^3 l_{2,0,0,1,1,1,0} m_b^2}{x} & f_{14}^l &= -\frac{(x-1)(x+1) \varepsilon^3 l_{1,1,0,0,0,1,2} m_b^2}{x} \\
f_{15}^l &= \frac{(x-1)^3(x+1) \varepsilon^2 l_{2,0,1,2,0,1,0} m_b^4}{x^2} & f_{16}^l &= \frac{(x-1)^2 \varepsilon^3 (2\varepsilon-1) l_{1,0,1,1,0,1,1} m_b^2}{x} \\
f_{17}^l &= -\frac{(x-1)(x+1) \varepsilon^4 l_{1,1,0,1,0,1,1} m_b^2}{x} \\
f_{18}^l &= \frac{(x-1)^2 \varepsilon^4 l_{1,1,0,1,0,1,1} m_b^2}{x} + \frac{(x-1)(x+3) \varepsilon^3 l_{0,2,0,1,0,1,1} m_b^2}{2x} \\
&\quad + \frac{(x-1)(x+3) \varepsilon^3 l_{1,1,0,0,0,1,2} m_b^2}{2x} + \frac{(x-1)^2 \varepsilon^2 l_{1,1,0,1,0,1,2} m_b^4}{2x} \tag{5.11} \\
f_1^m &= -\frac{(x-1)^2 \varepsilon^2 m_{0,0,0,1,2,2,0} m_b^2}{x} & f_2^m &= \frac{(x-1)^4 \varepsilon^2 m_{0,0,2,2,0,1,1} m_b^4}{x^2} \\
f_3^m &= -\frac{(x-1)(x+1) \varepsilon^3 m_{1,0,0,1,1,2,0} m_b^2}{x} & f_4^m &= \frac{(x-1)^3(x+1) \varepsilon^3 m_{1,0,2,1,0,1,1} m_b^4}{x^2}
\end{aligned}$$

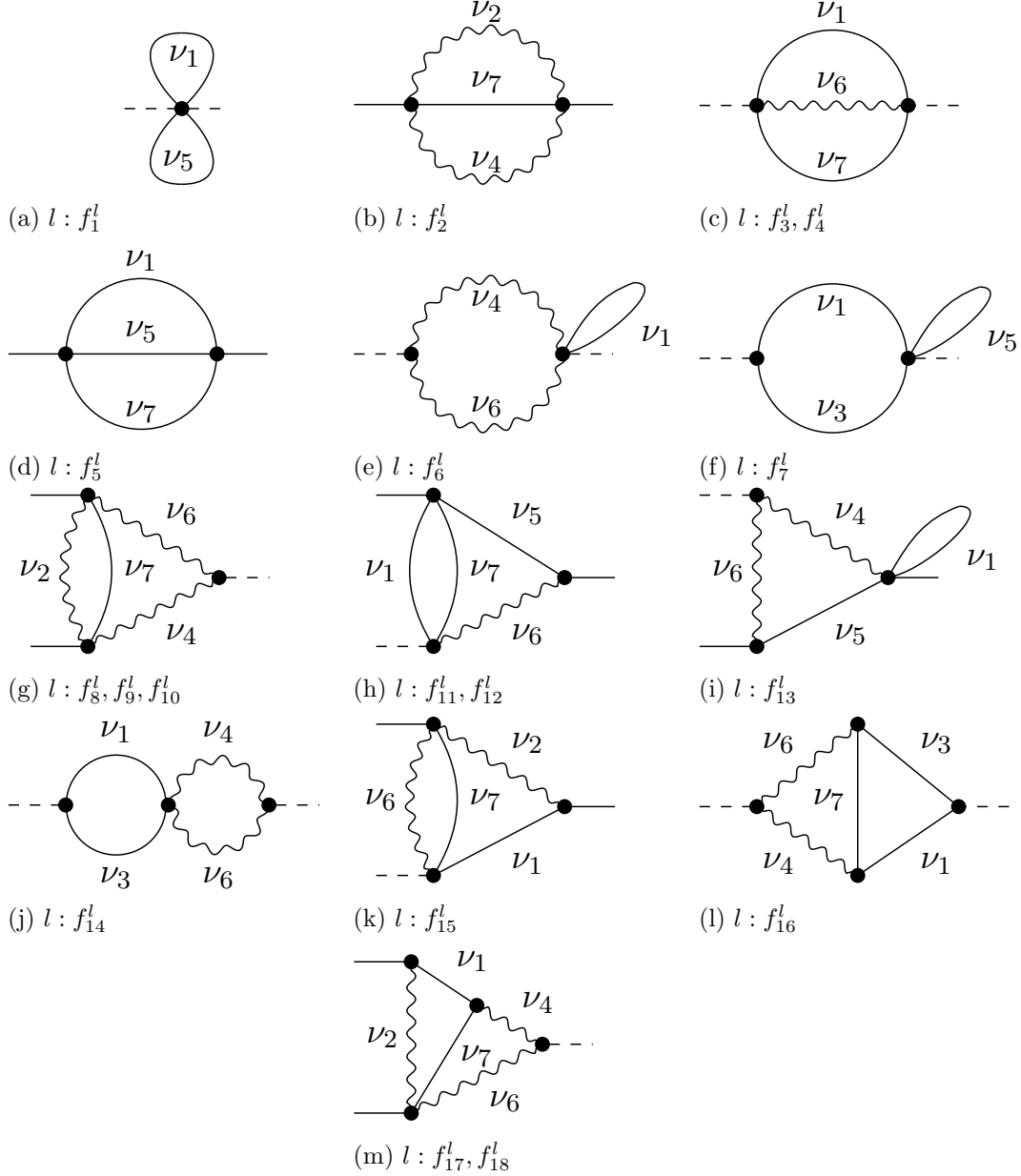


Figure 6: Scalar topologies contributing to $M_{y_t,2}^B$. The dashed line corresponds to the Higgs, wavy lines denote massless and continuous straight lines massive propagators. If a continuous straight line is external it carries momentum $p^2 = m_b^2$. The letters in the captions stand for the corresponding completed family l while the ν_i denote the relevant propagators.

$$f_5^m = -\frac{(x-1)(x+1)\varepsilon^4 m_{1,1,0,1,1,1,0} m_b^2}{x}$$

$$f_6^m = m_b^2 \left(\frac{2(x-1)^2 \varepsilon^4 m_{1,1,0,1,1,1,0}}{x} - \frac{(x-1)(3x-1)\varepsilon^3 m_{1,0,0,1,1,2,0}}{x} \right)$$

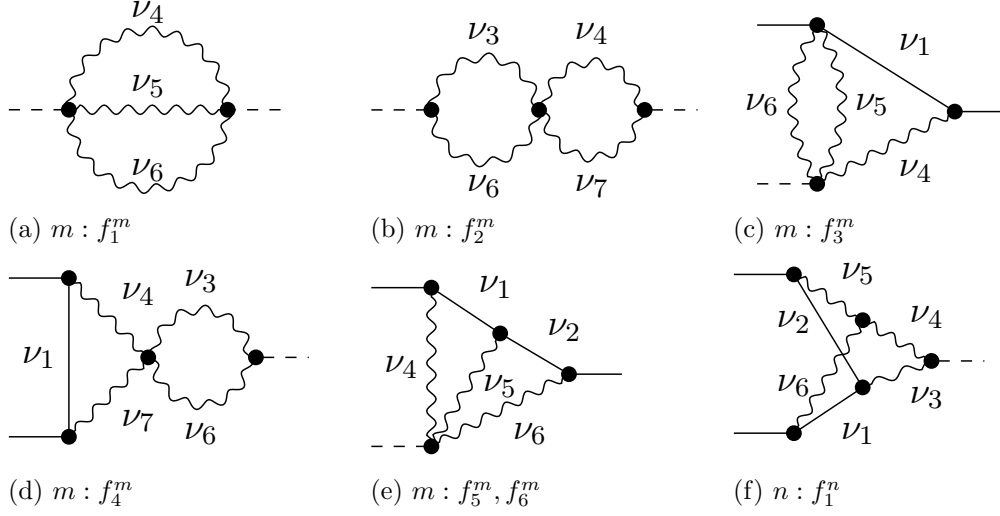


Figure 7: Scalar topologies contributing to $M_{y_t,2}^B$. The dashed line corresponds to the Higgs, wavy lines denote massless and continuous straight lines massive propagators. If a continuous straight line is external it carries momentum $p^2 = m_b^2$. The letters in the captions stand for the corresponding completed family m and n while the ν_i denote the relevant propagators.

$$-\frac{(x-1)^2 \varepsilon^2 (2\varepsilon+1) m_{1,1,0,1,2,1,0} m_b^4}{x} \quad (5.12)$$

$$f_1^n = \frac{(x-1)^3 (x+1) \varepsilon^4 n_{1,1,1,1,1,1,0} m_b^4}{x^2} \quad (5.13)$$

In order to compute the MIs we use the method of differential equation as described in paragraph 5.2. The large mass expansion of the MIs $(p_1 \cdot p_2) \ll m_b^2$ corresponding to the expansion $x \approx 1$ (see eq. (4.3)) is not as straightforward as for $gg \rightarrow H$. We therefore compute only the small subset

$$f_1^l = e^{2\gamma_E \varepsilon} \varepsilon^2 \Gamma(\varepsilon)^2 \quad (5.14)$$

$$f_2^l = \frac{e^{2\gamma_E \varepsilon} \varepsilon^3 \Gamma(-4\varepsilon) \Gamma(-\varepsilon)^2 \Gamma(\varepsilon) \Gamma(2\varepsilon)}{3\Gamma(-3\varepsilon) \Gamma(-2\varepsilon)} \quad (5.15)$$

$$f_6^l = -\frac{e^{2\gamma_E \varepsilon} \varepsilon^2 \left(\frac{x}{(x-1)^2}\right)^\varepsilon \Gamma(1-\varepsilon)^2 \Gamma(\varepsilon)^2}{\Gamma(1-2\varepsilon)} \quad (5.16)$$

$$\lim_{x \uparrow 1} f_{18}^l = \frac{\pi(x+3) e^{2\gamma_E \varepsilon} \varepsilon^3 \left(\frac{x}{(x-1)^2}\right)^{2\varepsilon} \Gamma\left(\frac{1}{2}-2\varepsilon\right) \Gamma(-\varepsilon) \Gamma(4\varepsilon) \Gamma\left(\varepsilon+\frac{1}{2}\right)}{2\sqrt{x} \Gamma(1-2\varepsilon) \Gamma(2\varepsilon)} \quad (5.17)$$

$$f_1^m = \frac{e^{2\gamma_E \varepsilon} \varepsilon^2 \left(\frac{x}{(x-1)^2}\right)^{2\varepsilon} \Gamma(1-\varepsilon) \Gamma(-\varepsilon)^2 \Gamma(2\varepsilon+1)}{\Gamma(1-3\varepsilon)} \quad (5.18)$$

$$f_2^m = \frac{e^{2\gamma_E \varepsilon} \pi 16^\varepsilon \varepsilon^2 (1-x)^{-4\varepsilon} x^{2\varepsilon} \Gamma(1-\varepsilon)^2 \Gamma(\varepsilon)^2}{\Gamma\left(\frac{1}{2}-\varepsilon\right)^2} \quad (5.19)$$

to all orders. Furthermore we need f_5^l for which we could not find a closed form but provide the Laurent coefficients, obtained from a direct integration with `HYPERINT`, in the ancillary material. With this input, all other boundary conditions can be obtained by imposing regularity conditions on the general solution at (pseudo-) thresholds in the s -channel. To determine if the particular solution of the differential equation for a given canonical integral has to be regular at either $s = 0$ or $s = 4m_b^2$ it suffices to know the leading singular behavior of all Feynman integrals appearing in its definition. This can be done by looking at all possible s -channel cuts of the graphs fig. 6 and fig. 7 or alternatively by performing an expansion by regions with tools like `FIESTA 4.1` or `asy.m` [71, 72]. In particular we use the exact boundary values

$$\lim_{x \uparrow 1} = f_8^l = \lim_{x \uparrow 1} f_{17}^l = \lim_{x \uparrow 1} f_5^m = 0 \quad (5.20)$$

augmented with the regularity condition at $s = 0$ ($x = 1$) of

$$\{f_l^3, f_l^4, f_l^7, f_l^8, f_l^{11}, f_l^{12}, f_l^{14}, f_l^{15}, f_l^{16}, f_l^{17}, f_m^5, f_n^1\}, \quad (5.21)$$

and the regularity at threshold $s = 4m_b^2$ ($x = -1$) of

$$\{f_l^8, f_l^9, f_l^{10}, f_l^{13}, f_l^{12}, f_m^3, f_m^4, f_m^5, f_m^6\}. \quad (5.22)$$

To impose regularity conditions, the general solution of the differential equation for the n th Laurent-coefficient of our canonical basis integrals has to be expanded around $x_1 = 1 - \delta$ and $x_{-1} = -1 + i\delta$ for $0 < \delta \ll 1$. We perform these expansions by rewriting the general solution as $H(\vec{a}, \delta)$ with the help of `HYPERINT` and extract the $\log(\delta)$ -singularities as discussed in section 4 around both $x_{\pm 1}$. For integrals regular at these points the coefficients in front of $\log(\delta)$ have to vanish. We thus obtain a over-determined system of equations for the boundary constants. To fix all boundary values at $\mathcal{O}(\varepsilon^n)$ we need to perform $n+2$ iterated integrations. All 25 Feynman integrals can be expressed in terms of harmonic polylogarithms eq. (4.6) in the variable $x(s/m_b^2)$ eq. (4.5) and are provided up to weight six in the ancillary material. We checked the integrals for all kinematic regimes numerical against `FIESTA 4.1`.

6 Conclusion

We have presented two two-loop amplitudes up to order $\mathcal{O}(\varepsilon^2)$ relevant for improving state of the art Higgs observable predictions. The first is the two-loop amplitude for the gluon fusion production process, which was previously only known to finite order. The result we provide will allow the subtraction of the infrared poles of the three-loop double virtual amplitudes in the NNLO prediction. The second amplitude we obtained was the two loop amplitude for the Higgs boson decay to a pair of bottom quarks through the Higgs to gluon coupling in the HEFT, effectively describing top-Yukawa-induced virtual corrections up to $\mathcal{O}(\alpha_s^3)$.

We have derived canonical bases for the integral families relevant for both calculations, which will allow the systematic calculation of higher orders in ε should they be required. We have checked the results obtained for the integrals numerically against sector-decomposition programs and we have compared the pieces of our amplitude against existing results when available.

Although they do not constitute physical observables in themselves, our results can be combined with other components to improve the predictions on the production and decay rates of the Higgs boson and we hope to combine them to future results to further our understanding of its properties.

Acknowledgments

We are greatly indebted to R. Gauld, V. Hirschi, F. Moriello and A. Penin for many fruitful discussions. This project has received funding from the European Research Council (ERC) under grant agreement No 694712 (PertQCD) and the Swiss National Science Foundation (SNF) under contract agreements No 177632 and 179016.

Appendix A Tensor basis for the $H \rightarrow b\bar{b}$ amplitude

In section 3, we claimed that the bare amplitude amputated from its external spinor could be decomposed in a basis of Dirac matrices as follows:

$$\mathcal{M}^0(p_1, p_2) = \text{Id } M_0^0 + (\not{p}_1 - m_b)M_1^0 + (\not{p}_2 + m_b)M_2^0 + (\not{p}_1 - m_b)(\not{p}_2 + m_b)M_{12}^0, \quad (\text{A.1})$$

This decomposition is manifest by decomposing \mathcal{M} as a linear combination of Dirac matrices contracted with tensor integrals:

$$\mathcal{M}^0(p_1, p_2) = \sum_i \Gamma_i^{[\mu]_i}(p_1, p_2) I_{[\mu]_i}(p_1, p_2), \quad (\text{A.2})$$

where $[\mu]_i$ are a collection of Lorentz indices, the $I_{[\mu]_i}(p_1, p_2)$ are tensorial integrals and $\Gamma_i^{[\mu]_i}(p_1, p_2)$ is a product of Dirac-space matrices which overall has Lorentz indices $[\mu]_i$ and is built from the identity, basic Dirac matrices γ^μ , \not{p}_1 and \not{p}_2 . Furthermore the tensorial integrals can be decomposed as a linear combination of scalar functions multiplied with tensors obtained from products of the Lorentz metric $g_{\mu\nu}$, and the momenta p_1^μ and p_2^μ . As a result, we can write

$$\mathcal{M}^0 = \sum_j \Gamma_j(p_1, p_2) I_j, \quad (\text{A.3})$$

where I_j are scalar integrals and $\Gamma_j(p_1, p_2)$ are products of \not{p}_1 , \not{p}_2 and a number of basic Dirac matrices whose Lorentz indices are contracted with each other. Solving the algebra, the Γ_j are linear combinations of products of \not{p}_1 and \not{p}_2 , which we can reduce using anticommutation relations as linear combinations of the four Dirac matrices of eq. (A.1).

References

- [1] **CMS** Collaboration, A. M. Sirunyan *et al.*, *Combined measurements of Higgs boson couplings in proton–proton collisions at $\sqrt{s} = 13$ TeV*, *Eur. Phys. J.* **C79** (2019), no. 5 421, [[1809.10733](#)].
- [2] **ATLAS** Collaboration, G. Aad *et al.*, *Combined measurements of Higgs boson production and decay using up to 80 fb⁻¹ of proton-proton collision data at $\sqrt{s} = 13$ TeV collected with the ATLAS experiment*, [1909.02845](#).
- [3] **CMS** Collaboration, A. M. Sirunyan *et al.*, *Measurement and interpretation of differential cross sections for Higgs boson production at $\sqrt{s} = 13$ TeV*, *Phys. Lett.* **B792** (2019) 369–396, [[1812.06504](#)].
- [4] **ATLAS** Collaboration, T. A. collaboration, *Combined measurement of the total and differential cross sections in the $H \rightarrow \gamma\gamma$ and the $H \rightarrow ZZ^* \rightarrow 4\ell$ decay channels at $\sqrt{s} = 13$ TeV with the ATLAS detector*, .
- [5] C. Anastasiou, C. Duhr, F. Dulat, E. Furlan, T. Gehrmann, F. Herzog, A. Lazopoulos, and B. Mistlberger, *High precision determination of the gluon fusion Higgs boson cross-section at the LHC*, *JHEP* **05** (2016) 058, [[1602.00695](#)].
- [6] F. Dulat, B. Mistlberger, and A. Pelloni, *Precision predictions at N³LO for the Higgs boson rapidity distribution at the LHC*, *Phys. Rev.* **D99** (2019), no. 3 034004, [[1810.09462](#)].
- [7] L. Cieri, X. Chen, T. Gehrmann, E. W. N. Glover, and A. Huss, *Higgs boson production at the LHC using the q_T subtraction formalism at N³LO QCD*, *JHEP* **02** (2019) 096, [[1807.11501](#)].
- [8] C. Anastasiou, S. Beerli, S. Bucherer, A. Daleo, and Z. Kunszt, *Two-loop amplitudes and master integrals for the production of a Higgs boson via a massive quark and a scalar-quark loop*, *JHEP* **01** (2007) 082, [[hep-ph/0611236](#)].
- [9] A. Pak, M. Rogal, and M. Steinhauser, *Finite top quark mass effects in NNLO Higgs boson production at LHC*, *JHEP* **02** (2010) 025, [[0911.4662](#)].
- [10] R. V. Harlander, H. Mantler, S. Marzani, and K. J. Ozeren, *Higgs production in gluon fusion at next-to-next-to-leading order QCD for finite top mass*, *Eur. Phys. J.* **C66** (2010) 359–372, [[0912.2104](#)].
- [11] S. P. Jones, M. Kerner, and G. Luisoni, *Next-to-Leading-Order QCD Corrections to Higgs Boson Plus Jet Production with Full Top-Quark Mass Dependence*, *Phys. Rev. Lett.* **120** (2018), no. 16 162001, [[1802.00349](#)].

- [12] **CMS Collaboration** Collaboration, A. M. Sirunyan *et al.*, *Sensitivity projections for Higgs boson properties measurements at the HL-LHC*, Tech. Rep. CMS-PAS-FTR-18-011, CERN, Geneva, 2018.
- [13] **ATLAS Collaboration** Collaboration, G. Aad *et al.*, *Prospects for differential cross-section measurements of Higgs boson production measured in decays to ZZ and $\gamma\gamma$ with the ATLAS experiment at the High-Luminosity LHC*, Tech. Rep. ATL-PHYS-PUB-2018-040, CERN, Geneva, Dec, 2018.
- [14] J. Davies, R. Gröber, A. Maier, T. Rauh, and M. Steinhauser, *Top quark mass dependence of the Higgs boson-gluon form factor at three loops*, *Phys. Rev.* **D100** (2019), no. 3 034017, [[1906.00982](#)].
- [15] R. V. Harlander, M. Prausa, and J. Usovitsch, *The light-fermion contribution to the exact Higgs-gluon form factor in QCD*, [1907.06957](#).
- [16] M. Czakon and M. Niggetiedt, *Exact quark-mass dependence of the Higgs-gluon form factor at three loops in QCD*, [2001.03008](#).
- [17] R. Bonciani, V. Del Duca, H. Frellesvig, J. M. Henn, F. Moriello, and V. A. Smirnov, *Two-loop planar master integrals for Higgs \rightarrow 3 partons with full heavy-quark mass dependence*, *JHEP* **12** (2016) 096, [[1609.06685](#)].
- [18] R. Bonciani, V. Del Duca, H. Frellesvig, J. M. Henn, M. Hidding, L. Maestri, F. Moriello, G. Salvatori, and V. A. Smirnov, *Evaluating two-loop non-planar master integrals for Higgs + jet production with full heavy-quark mass dependence*, [1907.13156](#).
- [19] H. Frellesvig, M. Hidding, L. Maestri, F. Moriello, and G. Salvatori, *The complete set of two-loop master integrals for Higgs + jet production in QCD*, [1911.06308](#).
- [20] **CMS Collaboration**, A. M. Sirunyan *et al.*, *Observation of Higgs boson decay to bottom quarks*, *Phys. Rev. Lett.* **121** (2018), no. 12 121801, [[1808.08242](#)].
- [21] **ATLAS Collaboration**, M. Aaboud *et al.*, *Observation of $H \rightarrow b\bar{b}$ decays and VH production with the ATLAS detector*, *Phys. Lett.* **B786** (2018) 59–86, [[1808.08238](#)].
- [22] **HL/HE WG2 group** Collaboration, M. Cepeda *et al.*, *Higgs Physics at the HL-LHC and HE-LHC*, [1902.00134](#).
- [23] G. Ferrera, G. Somogyi, and F. Tramontano, *Associated production of a Higgs boson decaying into bottom quarks at the LHC in full NNLO QCD*, *Phys. Lett.* **B780** (2018) 346–351, [[1705.10304](#)].

- [24] F. Caola, G. Luisoni, K. Melnikov, and R. Röntsch, *NNLO QCD corrections to associated WH production and $H \rightarrow b\bar{b}$ decay*, *Phys. Rev.* **D97** (2018), no. 7 074022, [[1712.06954](#)].
- [25] G. Ferrera, M. Grazzini, and F. Tramontano, *Associated WH production at hadron colliders: a fully exclusive QCD calculation at NNLO*, *Phys. Rev. Lett.* **107** (2011) 152003, [[1107.1164](#)].
- [26] J. M. Campbell, R. K. Ellis, and C. Williams, *Associated production of a Higgs boson at NNLO*, *JHEP* **06** (2016) 179, [[1601.00658](#)].
- [27] C. Anastasiou, F. Herzog, and A. Lazopoulos, *The fully differential decay rate of a Higgs boson to bottom-quarks at NNLO in QCD*, *JHEP* **03** (2012) 035, [[1110.2368](#)].
- [28] V. Del Duca, C. Duhr, G. Somogyi, F. Tramontano, and Z. Trócsányi, *Higgs boson decay into b -quarks at NNLO accuracy*, *JHEP* **04** (2015) 036, [[1501.07226](#)].
- [29] F. Herzog, B. Ruijl, T. Ueda, J. A. M. Vermaseren, and A. Vogt, *On Higgs decays to hadrons and the R -ratio at N^4LO* , *JHEP* **08** (2017) 113, [[1707.01044](#)].
- [30] R. Mondini, M. Schiavi, and C. Williams, *N^3LO predictions for the decay of the Higgs boson to bottom quarks*, *JHEP* **06** (2019) 079, [[1904.08960](#)].
- [31] W. Bernreuther, L. Chen, and Z.-G. Si, *Differential decay rates of CP -even and CP -odd Higgs bosons to top and bottom quarks at NNLO QCD*, *JHEP* **07** (2018) 159, [[1805.06658](#)].
- [32] A. Behring and W. Bizon, *Higgs decay into massive b -quarks at NNLO QCD in the nested soft-collinear subtraction scheme*, [1911.11524](#).
- [33] A. Primo, G. Sasso, G. Somogyi, and F. Tramontano, *Exact Top Yukawa corrections to Higgs boson decay into bottom quarks*, *Phys. Rev.* **D99** (2019), no. 5 054013, [[1812.07811](#)].
- [34] J. Alwall, R. Frederix, S. Frixione, V. Hirschi, F. Maltoni, O. Mattelaer, H. S. Shao, T. Stelzer, P. Torrielli, and M. Zaro, *The automated computation of tree-level and next-to-leading order differential cross sections, and their matching to parton shower simulations*, *JHEP* **07** (2014) 079, [[1405.0301](#)].
- [35] P. Nogueira, *Automatic Feynman graph generation*, *J. Comput. Phys.* **105** (1993) 279–289.
- [36] J. A. M. Vermaseren, *New features of FORM*, [math-ph/0010025](#).
- [37] K. G. Chetyrkin and F. V. Tkachov, *Integration by Parts: The Algorithm to Calculate beta Functions in 4 Loops*, *Nucl. Phys.* **B192** (1981) 159–204.

- [38] F. V. Tkachov, *A Theorem on Analytical Calculability of Four Loop Renormalization Group Functions*, *Phys. Lett.* **100B** (1981) 65–68.
- [39] C. Anastasiou and A. Lazopoulos, *Automatic integral reduction for higher order perturbative calculations*, *JHEP* **07** (2004) 046, [[hep-ph/0404258](#)].
- [40] P. Maierhöfer and J. Usovitsch, *Kira 1.2 Release Notes*, [1812.01491](#).
- [41] N. Deuschmann, C. Duhr, F. Maltoni, and E. Vryonidou, *Gluon-fusion Higgs production in the Standard Model Effective Field Theory*, *JHEP* **12** (2017) 063, [[1708.00460](#)]. [Erratum: JHEP02,159(2018)].
- [42] F. Dulat, A. Lazopoulos, and B. Mistlberger, *iHixs 2 — Inclusive Higgs cross sections*, *Comput. Phys. Commun.* **233** (2018) 243–260, [[1802.00827](#)].
- [43] Z. Kunszt, A. Signer, and Z. Trocsanyi, *Singular terms of helicity amplitudes at one loop in QCD and the soft limit of the cross-sections of multiparton processes*, *Nucl. Phys.* **B420** (1994) 550–564, [[hep-ph/9401294](#)].
- [44] S. Catani, S. Dittmaier, and Z. Trocsanyi, *One loop singular behavior of QCD and SUSY QCD amplitudes with massive partons*, *Phys. Lett.* **B500** (2001) 149–160, [[hep-ph/0011222](#)].
- [45] J. C. Collins, F. Wilczek, and A. Zee, *Low-Energy Manifestations of Heavy Particles: Application to the Neutral Current*, *Phys. Rev.* **D18** (1978) 242.
- [46] C. Anastasiou, C. Duhr, F. Dulat, F. Herzog, and B. Mistlberger, *Higgs Boson Gluon-Fusion Production in QCD at Three Loops*, *Phys. Rev. Lett.* **114** (2015) 212001, [[1503.06056](#)].
- [47] M. Spira, A. Djouadi, D. Graudenz, and P. M. Zerwas, *Higgs boson production at the LHC*, *Nucl. Phys.* **B453** (1995) 17–82, [[hep-ph/9504378](#)].
- [48] C. Duhr and F. Dulat, *PolyLogTools - Polylogs for the masses*, [1904.07279](#).
- [49] C. Anastasiou and C. Specchia, *One-loop QCD contributions to differential cross-sections for Higgs production at $N^3\text{LO}$* , *JHEP* **05** (2019) 080, [[1812.05857](#)].
- [50] T. Inami, T. Kubota, and Y. Okada, *Effective Gauge Theory and the Effect of Heavy Quarks in Higgs Boson Decays*, *Z. Phys.* **C18** (1983) 69–80.
- [51] K. G. Chetyrkin, B. A. Kniehl, and M. Steinhauser, *Virtual top quark effects on the $H \rightarrow \bar{c} b$ anti- b decay at next-to-leading order in QCD*, *Phys. Rev. Lett.* **78** (1997) 594–597, [[hep-ph/9610456](#)].

- [52] K. G. Chetyrkin, B. A. Kniehl, and M. Steinhauser, *Three loop $O(\alpha_s^{**2} G(F) M(t)^{**2})$ corrections to hadronic Higgs decays*, *Nucl. Phys.* **B490** (1997) 19–39, [[hep-ph/9701277](#)].
- [53] K. G. Chetyrkin, *Four-loop renormalization of QCD: Full set of renormalization constants and anomalous dimensions*, *Nucl. Phys.* **B710** (2005) 499–510, [[hep-ph/0405193](#)].
- [54] C. Anastasiou and A. Penin, *Light Quark Mediated Higgs Boson Threshold Production in the Next-to-Leading Logarithmic Approximation*, [2004.03602](#).
- [55] E. Remiddi and J. A. M. Vermaseren, *Harmonic polylogarithms*, *Int. J. Mod. Phys.* **A15** (2000) 725–754, [[hep-ph/9905237](#)].
- [56] D. Maitre, *HPL, a mathematica implementation of the harmonic polylogarithms*, *Comput. Phys. Commun.* **174** (2006) 222–240, [[hep-ph/0507152](#)].
- [57] D. Maitre, *Extension of HPL to complex arguments*, *Comput. Phys. Commun.* **183** (2012) 846, [[hep-ph/0703052](#)].
- [58] E. Panzer, *Algorithms for the symbolic integration of hyperlogarithms with applications to Feynman integrals*, *Comput. Phys. Commun.* **188** (2015) 148–166, [[1403.3385](#)].
- [59] A. V. Kotikov, *Differential equations method: New technique for massive Feynman diagrams calculation*, *Phys. Lett.* **B254** (1991) 158–164.
- [60] T. Gehrmann and E. Remiddi, *Differential equations for two loop four point functions*, *Nucl. Phys.* **B580** (2000) 485–518, [[hep-ph/9912329](#)].
- [61] J. M. Henn, *Multiloop integrals in dimensional regularization made simple*, *Phys. Rev. Lett.* **110** (2013) 251601, [[1304.1806](#)].
- [62] K.-T. Chen, *Iterated path integrals*, *Bull. Amer. Math. Soc.* **83** (09, 1977) 831–879.
- [63] A. B. Goncharov, *Multiple polylogarithms, cyclotomy and modular complexes*, *Math. Res. Lett.* **5** (1998) 497–516, [[1105.2076](#)].
- [64] U. Aglietti, R. Bonciani, G. Degrossi, and A. Vicini, *Analytic Results for Virtual QCD Corrections to Higgs Production and Decay*, *JHEP* **01** (2007) 021, [[hep-ph/0611266](#)].
- [65] R. Bonciani, P. Mastrolia, and E. Remiddi, *Master integrals for the two loop QCD virtual corrections to the forward backward asymmetry*, *Nucl. Phys.* **B690** (2004) 138–176, [[hep-ph/0311145](#)].

- [66] R. Bonciani, P. Mastrolia, and E. Remiddi, *Vertex diagrams for the QED form-factors at the two loop level*, *Nucl. Phys.* **B661** (2003) 289–343, [[hep-ph/0301170](#)]. [Erratum: *Nucl. Phys.*B702,359(2004)].
- [67] J. Ellis, *TikZ-Feynman: Feynman diagrams with TikZ*, *Comput. Phys. Commun.* **210** (2017) 103–123, [[1601.05437](#)].
- [68] R. N. Lee, *LiteRed 1.4: a powerful tool for reduction of multiloop integrals*, *J. Phys. Conf. Ser.* **523** (2014) 012059, [[1310.1145](#)].
- [69] C. W. Bauer, A. Frink, and R. Kreckel, *Introduction to the GiNaC framework for symbolic computation within the C++ programming language*, *J. Symb. Comput.* **33** (2000) 1, [[cs/0004015](#)].
- [70] J. Vollinga and S. Weinzierl, *Numerical evaluation of multiple polylogarithms*, *Comput. Phys. Commun.* **167** (2005) 177, [[hep-ph/0410259](#)].
- [71] A. Pak and A. Smirnov, *Geometric approach to asymptotic expansion of Feynman integrals*, *Eur. Phys. J.* **C71** (2011) 1626, [[1011.4863](#)].
- [72] B. Jantzen, A. V. Smirnov, and V. A. Smirnov, *Expansion by regions: revealing potential and Glauber regions automatically*, *Eur. Phys. J.* **C72** (2012) 2139, [[1206.0546](#)].